HIGH-PASS FILTERING OF SMALL SIGNALS BY THE ROD NETWORK IN THE RETINA OF THE TOAD, *BUFO MARINUS*

V. TORRE AND W. G. OWEN
The Physiological Laboratory, University of Cambridge, Cambridge, United Kingdom

ABSTRACT The electrical spread of excitation in the network of rod photoreceptors was studied by intracellular recording in the isolated, perfused retina of the toad, *Bufo marinus*. Experiments with dim, bar-shaped flashes of light revealed that the rod network behaves as a high-pass filter to laterally propagating small signals. Such a behavior had been found earlier in the turtle (Detwiler et al., 1980). Three electrical equivalent circuit models that can explain this behavior were considered and analytical solutions to the network equations were obtained. By fitting these analytical expressions to linear responses elicited by weak light flashes and to voltage excursions elicited by extrinsic current injections, values for the circuit parameters were determined. Values obtained by independent methods were consistent. The effects of changing each of these parameters in turn upon the high-pass filtering of small signals were then predicted. These predictions provided a framework for an analysis of the ionic basis of the underlying mechanism, which is described in the following paper.

INTRODUCTION

It is now well established that rod photoreceptors in the retinae of many species of lower vertebrates are coupled together via electrical junctions (Schwartz, 1975, 1976; Fain, 1975, 1976; Copenhagen and Owen, 1976*a*,*b*; Detwiler et al., 1978, 1980; Werblin, 1978; Gold, 1979; Attwell and Wilson, 1980). Electrical coupling of cones was earlier demonstrated by Baylor et al. (1971) and subsequently analyzed in terms of an electrical circuit model in which each cone of a two-dimensional array was represented by a resistor and capacitor in parallel (Lamb and Simon, 1976; Detwiler and Hodgkin, 1979). Although this model accounted satisfactorily for the electrical coupling of cones, it was recently shown that the responses of rods to spatially structured, weak stimuli cannot be accounted for in the same way (Detwiler et al., 1978, 1980). This is because the rod network behaves as a high-pass filter to laterally propagating currents, a behavior that Detwiler et al. described in terms of an equivalent two-dimensional circuit in which each rod was represented by a transverse element containing an inductance.

In the present paper, we apply this model to an analysis of the spread of excitation between rods of the toad, *Bufo marinus*. Our purpose is to establish reliable values for the network parameters as they apply under normal physiological conditions. In the following paper, the effects on the network parameters of external ion substitutions will be analyzed.

METHODS

Experiments were performed on the isolated, perfused retina of the toad, *Bufo marinus*. After dark-adapting overnight, a toad was pithed and its eyes removed under deep red light. All subsequent procedures were carried out under infrared illumination with the aid of an infrared image converter (FJW Industries, Inc., Mt. Prospect, IL). Using a razor blade and dissecting scissors, we hemisected the eye sagitally just posterior to the *ora serrata*. The eyecup, containing the retina, was then divided into three segments with a razor blade. The optic disk was discarded and the segments were transferred to a Petri dish containing oxygenated control Ringer's solution (see below). The retina was gently peeled away from the retinal pigmented epithelium (RPE) with fine forceps and laid, receptor side up, on a 1-cm-diam disk of filter paper. A second paper disk of the same size, but with a 3-mm-diam hole cut at its center, was placed over the first so that the center of the retinal segment was exposed, but its periphery was sandwiched between the disks. By briefly touching the underside of the lower disk to some filter paper, we drained the space between retina and lower disk, and a satisfactory mechanical adhesion was obtained.

Thus mounted, the retina was placed in a perfusion chamber and clamped tightly in position. The chamber was in turn clamped to an *X-Y* table in a light-tight Faraday cage. The perfusion medium flowed under gravity over the retina with a flow rate of 2–3 ml/min.

Perfusion Medium

Retinae were perfused with a control Ringer's solution whose ionic composition was as follows: 132 mM Na^+, 2.6 mM K^+, 120.6 mM Cl^-, 22 mM HCO_3^-, 2 mM Ca^{++}, 2 mM Mg^{++}, and 5 mM glucose. The solution was buffered to pH 7.8 by bubbling with a mixture of 95% O_2 and 5% CO_2.

Dr. Torre's present address is Istituto di Scienze Fisiche, Viale Benedetto XV 5, Genoa, Italy.
Dr. Owen's present address is Department of Biophysics & Medical Physics, University of California, Berkeley, CA 94720.
Address all correspondence to Dr. Owen.

Optical Stimulation

Stimuli were presented using a two-beam optical stimulator, virtually identical with that described by Baylor and Hodgkin (1973). An additional beam-splitting prism in a specially built mount allowed light to be delivered vertically to the preparation and simultaneously allowed light from the preparation to pass back through the final microscope objective to an infrared sensitive TV camera. Thus, by illuminating the preparation with infrared light, stimuli could be focused and the alignment between electrode and stimulus optimized during the course of the experiment.

Stimuli were either diffuse or consisted of the reduced image of a long, narrow slit projected onto the retina. In the plane of the retina, the slit-shaped stimulus measured 11 μm wide by 1 mm long. Stimulus intensity was calibrated regularly using a photodiode. The optical densities of neutral filters and of interference filters at their peak transmission wavelengths were also periodically checked.

Electrical Recording and Data Storage

Intracellular potentials were recorded using fine glass micropipettes filled with 4 M K-acetate, introduced into the retina by a stepping hydraulic microadvancer (David Kopf Instruments, Tujunga, CA). Potentials were amplified by a field effect transistor input preamplifier (model 701; W-P Instruments, Inc., New Haven, CT) followed by a DC high-gain amplifier. The amplified signal was displayed on a storage oscilloscope and a chart recorder, and stored on magnetic tape (Philips FM instrumentation recorder; Philips Electronic Instruments, Inc., Mahwah, NJ). The frequency bandwidth of the recorder at the tape speed used was 0–300 Hz. The reference against which intracellular potentials were measured was a calomel electrode connected by a 3-M KCl bridge to a well in the perfusion chamber also containing 3 M KCl. This was connected, in turn, by a Ringer's solution-agar bridge to a second well into which the Ringer's solution drained before flowing under gravity to a waste-collecting bottle. This arrangement ensured that liquid-junction potentials were minimized.

Current Injection

In some experiments, current was injected intracellularly while simultaneously monitoring intracellular potential. Double-barreled electrodes were used for these experiments. They were prepared according to the technique described by Brown and Flaming (1977). Current was injected using the current-injection circuit of the amplifier.

Because of the difficulty in eliminating secondary paths for current flow to ground through the perfusion system, it proved impossible to monitor injected currents using a current-voltage converter in the ground return as we would have preferred. Instead, we calibrated our current-injection circuit by passing current through microelectrodes into a dish of control Ringer's solution in the ground return of which was a current-voltage converter. Simultaneously, we calibrated the current monitor output of the preamplifier unit against the output of the current-voltage converter. Neither calibration changed when (*a*) we increased the circuit load by adding a 200-MΩ resistance in the ground return, and (*b*) the electrode was broken so that its impedance became negligible. Thus, the current-passing circuit was unaffected by its load and we were able to rely on our calibrated values of the injected current.

Correction for Capacitive Transients

In experiments involving high-impedance, double-barreled electrodes for the injection of extrinsic current, the voltage record is generally contaminated by a transient that occurs at the onset and offset of the current pulse. Because we were interested in the time course of the change in membrane potential, this artifact had to be eliminated. We did this by recording the artifact resulting from injection of each of the experimental currents with the electrode in the external medium and then digitally

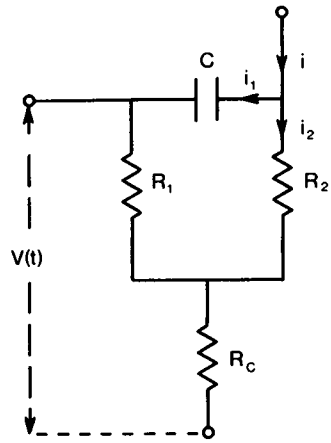

FIGURE 1 Equivalent circuit of a double-barreled electrode. R_1 and R_2 are the resistances of voltage-recording and current-injecting barrels, respectively. C is the interbarrel capacitance and R_c the coupling resistance. $V(t)$ is the voltage artifact recorded when a pulse of current (i) is passed through the current-passing barrel.

subtracting the appropriate artifact from each of the intracellular voltage records. Our justification for this procedure is as follows: (*a*) The equivalent circuit of the double-barreled electrode is shown in Fig. 1. R_1 and R_2 represent the resistance of voltage-recording and current-injecting barrels, respectively. C is the interbarrel capacitance. R_c is the coupling resistance of the electrode. (*b*) The artifact in the voltage record during injection of a DC-current step is the result of the capacitive current, i_1, flowing to ground across R_1 and R_c and the remainder of the injected current, i_2, flowing across R_c. Thus, the voltage artifact, $V(t)$, is given by:

$$V(t) = (i_1 + i_2)R_c + i_1R_1$$

$$= iR_c + i_1R_1,$$

where $i(=i_1 + i_2)$ is the total injected current, but $(i - i_1)R_2 = i_1R_1 + 1/c \int i_1 dt$ or $iR_2/R_1 + R_2 = i_1 + [1/c(R_1 + R_2)] \int i_1 dt$. The solution for a step change in current is easily shown to be

$$i_1 = \frac{iR_2}{(R_1 + R_2)} \cdot e^{-t/(R_1+R_2)C}.$$

Thus,

$$V(t) = iR_c + \frac{iR_2}{(R_1 + R_2)} \cdot e^{-t/(R_1+R_2)C}.$$

Note that the time-dependent term is independent of R_c and cannot be affected by resistances added in series with R_c. Thus, the magnitude of the voltage artifact should not change as the electrode enters a cell. Because the value of the coupling resistance, R_c, depends upon the free volume of external electrolyte shared by the two barrels and upon the conductivity of the external electrolyte, it is possible that upon entering the internal environment of the cell, R_c may change. This, however, will only affect the DC component of the artifact; the magnitude and time course of the capacitive transient will be unchanged. Thus, subtraction of the voltage artifact measured in the extracellular medium from the intracellularly recorded voltage change should correct for the capacitive transient, but may undercorrect for the DC component. While there must remain some uncertainty in our measured values of input impedance, therefore, the time-dependence of the input impedance should be accurately revealed. Moreover, by selecting electrodes whose coupling resistances are small compared with the input impedance of the network, the error in the absolute value will be minimized. For this reason, we rejected all

electrodes with a coupling resistance $\gtrsim 10^{-1}$ of measured input impedances.

We typically used electrodes having a coupling resistance of 2–5 MΩ, though we occasionally accepted values up to 10 MΩ. Electrodes with coupling resistances $\gtrsim$10 MΩ and/or with transient artifacts whose total duration was $\gtrsim$100 ms were rejected. Furthermore, if either of these parameters were found to have changed by more than ~15% during the course of an experiment, the data were discarded. Because the coupling resistance measured in Ringer's solution was generally at least one, and often nearly two, orders of magnitude smaller than the input resistance of the network, we believe that any systematic error in our estimates of membrane impedances that might result from this procedure is likely to be small.

Data Reduction

The data, stored in analogue form on magnetic tape, were replayed and digitized, usually at a sampling frequency of 50 Hz (one point every 20 ms). In some experiments a faster sampling rate was required to preserve adequate resolution. In such cases the sampling rate used is specified in the appropriate figure legend.

All signals were filtered before analog-to-digital (A-D) conversion by a 6-pole Butterworth low-pass filter (corner frequency 100 Hz). Slow responses were additionally smoothed after A-D conversion by a digital filter of the following type: Defining successive points as $x(t - N\Delta t)$, $x[t - (N - 1)\Delta t], \ldots x(t), \ldots x[t + (N - 1)\Delta t], x(t + N\Delta t)$, where Δt is the interval between each point, we smooth by calculating a running mean, thus

$$\tilde{x} = \frac{1}{(2N + 1)} \Big| x(t - N\Delta t) + x[t - (N - 1)\Delta t] + \ldots x(t) + \ldots x(t + N\Delta t) \Big| . \quad (1)$$

This is a common procedure described, for example, in Bendat and Piersol (1971). Appropriate choice of the value of N defines the time window over which the running mean is calculated. The transfer function of such a filter is given by

$$H(f) = \frac{1}{(2N + 1)} + \frac{2}{(2N + 1)} \sum_{1}^{N} {}_{k} \cos (2\pi f k \Delta t), \quad (2)$$

where f is the frequency.

Our procedure was successively to increase the value of N, starting from zero, until the response appeared sufficiently smooth, yet undistorted when compared with the unprocessed response. Of course, this procedure could only be used in the case of slow responses. When analyzing responses with rapid initial transients, as in the case of those elicited by bright stimuli or voltage changes elicited by steps of extrinsic current, we kept the value of N at zero (i.e., the data remained unsmoothed). In calculating values of the network length constant, λ, responses smoothed by the above procedure were used. A least-squares routine was used to compute the value of λ at various times during these responses.

Effective Cell Spacing of the Rod Network

To apply our model of the rod network to experimental data, it was important to obtain a reliable estimate of rod density in the retina of *Bufo marinus*. For this, we relied upon an histological cross section through the photoreceptor layer published by Fain (1976). The cross section covers an area 155 × 72.5 μm and contains 130 rods, one rod for every 86 μm^2 of retina. The apparent value of the mean cell spacing is thus 9.3 μm. However, some shrinkage inevitably occurs during histological preparation. Allowing for ~10% of linear shrinkage, we arrived at an effective cell spacing of 10 μm. This value was used in the analysis of all our data.

THEORETICAL ANALYSIS

We now consider three models, each of which can satisfactorily account for the high-pass filtering behavior of the rod network. Experiments justifying our consideration of linear models such as these are described at the beginning of the following section.

The rods are assumed to be interconnected in a square array (Lamb and Simon, 1976). Stimulating such an array with a unidimensional stimulus such as a long, narrow bar of light will constrain light-evoked currents to flow laterally, in a vector perpendicular to the stimulus. The analysis of experiments in which such stimuli are used can therefore be simplified by treating the network as unidimensional. In experiments involving radially symmetrical light stimuli or the point injection of extrinsic currents, however, a two-dimensional analysis must be carried out. In this section, we will derive analytical solutions of the circuit equations for both the unidimensional and the two-dimensional cases.

Model 1

It is well-known that under certain conditions a membrane that undergoes voltage-dependent conductance changes may behave as though its equivalent circuit contains an inductance (Cole and Baker, 1941; Hodgkin and Huxley, 1952; Detwiler et al., 1980). A time-varying, voltage-dependent K^+ conductance activated by depolarization, deactivated by hyperpolarization, can give rise to this type of behavior. So, too, can a time-varying, voltage-dependent Na^+ (or Ca^{++}) conductance activated by hyperpolarization, deactivated by depolarization (Detwiler et al., 1980). As Detwiler et al. (1980) pointed out, the electrical equivalent circuit in either case consists of an inductance, L, and series conductance, g_2, both of which are in parallel with a second conductance, g_1. This is shown as the transverse element in Fig. 2*a*. The circuit equation is thus

$$Lg_2\dot{I}_n + I_n = Lg_1g_2\dot{V}_n + V_n(g_1 + g_2), \quad (3)$$

where I_n is the current flowing across the membrane of rod n, and V_n is its

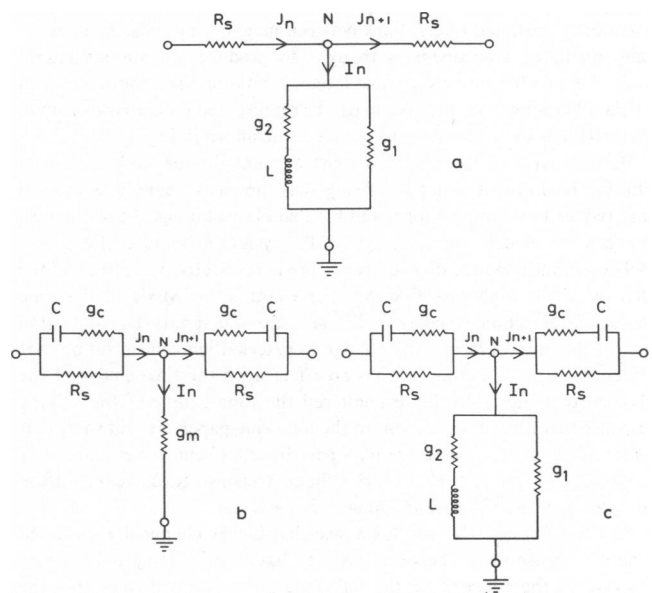

FIGURE 2 Equivalent circuits that can account for the high-pass filtering of small signals by the rod network. Light-evoked current spreads laterally through the shunting pathway, represented by the horizontal elements of the circuits, and leaks to ground across the plasma membrane of each rod in the array, represented by the vertical elements. The one-dimensional circuits shown here are appropriate when slit-shaped stimuli are used. Details of the circuits are given in the text.

transmembrane potential. Also

$$I_n = \frac{V_{n+1} + V_{n-1} - 2V_n}{R_s} + \tilde{I}_n, \tag{4}$$

where R_s is the shunt resistance between neighboring rods, and $\tilde{I}_n$ is the extrinsic current injected into rod n. This model is the one analyzed by Detwiler, et al. (1980) in their study of the rod network of the snapping turtle, *Chelydra serpentina*.

Model 2

High-pass filtering could result if the pathway coupling neighboring rods were not entirely resistive but behaved as though there were a capacitance in parallel with the shunting resistance, R_s, as illustrated in Fig. 2 *b*. This could reflect an intrinsic electrical property of the junctional membrane between neighboring rods or it might represent the action of a time-varying, voltage-dependent conductance in the pathway between the rods. The circuit equations, in this case, would be

$$I_n = g_m V_n \tag{5}$$

$$I_n = J_n - J_{n+1} \tag{6}$$

$$J_n - \frac{(V_n - V_{n-1})}{R_s} = C(\dot{V}_n - \dot{V}_{n-1}) - \frac{c}{g_c} J_n + \frac{c}{R_s g_c}(\dot{V}_n - \dot{V}_{n-1}). \tag{7}$$

Model 3

In this third model, suggested to us by Professor Sir Alan Hodgkin, the high-pass filtering involves a parallel combination of electrical and chemically mediated interactions between neighboring rods. The chemically mediated component is thought to produce a transient lateral excitation or, alternatively, a rapid lateral excitation that inactivates with a delay. In either case, the system can be represented for the case of small perturbations by the linear equivalent circuit shown in Fig. 2 *c*.

Because each of these models must account for the same high-pass filtering behavior, it is not surprising that the circuit equations in each case reduce to a common form and have similar solutions. To distinguish between the models, we must change the system in some artificial way and determine which of them correctly predicts the observed effects of the change on the high-pass filtering. For example, in Model 2 the time course of the voltage response to diffuse illumination must be identical to that of the photocurrent. Any change in external ion concentration that affects high-pass filtering but has no effect upon the time course of the photocurrent must also leave unaltered the time course of the voltage response to diffuse illumination. In the following paper, we will show that under all conditions where the high-pass filtering behavior is reduced or blocked, the time-to-peak of the voltage response to a weak, diffuse stimulus becomes significantly longer than normal.

Model 3 implies that any substance that blocks chemically mediated synaptic transmission between rods is likely to eliminate high-pass filtering by the network. In the following paper, we will show that the addition of up to 1 mM Co^{++} reduces, but does not abolish, high-pass filtering, a result that must weigh against that model. Thus, while we cannot eliminate conclusively any of these models, we believe that Model 1 most closely describes the underlying physiological mechanism. The analysis that follows is presented in terms of Model 1. It must be emphasized, however, that the analytical solutions obtained are equally applicable to the other models when appropriate changes in the parameters are made.

Spread of Excitation-Unidimensional Solution

In this treatment, rods lie in a linear array and are numbered $-n, \ldots -1, 0, +1 \ldots +n$. V_k is the voltage at rod k, I_k the current flowing into rod k, and J_k the current flowing laterally from rod k to rod $k+1$. Following the work of Detwiler et al. (1980), we describe in the following equation the lateral spread of excitation through such an array when the input is the voltage $V_0(t)$ at rod 0

$$A\dot{V} = -\tau BV - C. \tag{8}$$

A is an $(n \times n)$ matrix of the form

$$A = \begin{pmatrix} a1 & 0 & & \\ 1 & a & 1 & \\ 0 & 1 & a & 0 \\ & & & a1 \\ & & 0 & 1a \end{pmatrix},$$

where $a = -(g_l R_s + 2)$. B is an $(n \times n)$ matrix of the form

$$B = \begin{pmatrix} b1 & 0 & & \\ 1 & b & 1 & \\ 0 & 1 & b & 0 \\ & & & b1 \\ & & 0 & 1b \end{pmatrix},$$

where $b = -[(g_1 + g_2)R_s + 2]$. $\tau = 1/Lg_2$, and V and C are $n \times 1$ matrices: $V = [V_k(t), k = 1, \ldots n]$; $C = [C_1(t) = \tau V_0(t) + \dot{V}_0(t); C_k = 0, k = 2, \ldots n]$. Similarly, when the input is an extrinsic current, $I_1(t)$, injected into rod 1 of an array of n photoreceptors, the equations are

$$\bar{A}\dot{V} = -\tau \bar{B} V - \bar{C}; \tag{9}$$

τ and V are defined as for Eq. 8. The matrices $\bar{A}$ and $\bar{B}$ here have the form

$$\bar{A} = \begin{pmatrix} a2 & 0 & & \\ 1 & a & 1 & \\ 0 & 1 & a & 0 \\ & & & 1 \\ & & 0 & 1a \end{pmatrix}$$

$$\bar{B} = \begin{pmatrix} b2 & 0 & & \\ 1 & b & 1 & \\ 0 & 1 & b & 0 \\ & & & 1 \\ & & 0 & 1b \end{pmatrix}$$

and $\bar{C} = [C_1(t) = R_s[\tau I_1(t) + \dot{I}_1(t)]; C_k = 0\ k = 2, \ldots n]$. The solution of Eqs. 8 and 9 is the matrix $V(t)$. Details of the solution of Eqs. 8 and 9 are given in Appendix A.

The solution of Eq. 8 is

$$V_k(t) = \int_0^t h_k(t-\tau)V_0(\tau)d\tau, \tag{10}$$

where

$$h_k(t) = (-1)^k \frac{A_{n-k}}{A_n} \cdot \left[\delta(t) - \sum_1^n{}_m \frac{P_k[B_m^{(n)}]}{\prod_1^m{}_{j\neq m}[B_m^{(n)} - B_j^{(n)}]} \cdot e^{B_m^{(n)}t}\right]$$

$$= (-1)^k \frac{A_{n-k}}{A_n}\left[\delta(t) - \sum_1^n{}_m {}_kC_m^{(n)}\, e^{B_m^{(n)}t}\right],$$

where $\delta(t)$ is a Dirac delta function and

$$\frac{A_{n-k}}{A_n} = \frac{\prod_1^{n-k}{}_m\left(a - 2\cos\frac{m\pi}{n-k+1}\right)}{\prod_1^n{}_m\left(a - 2\cos\frac{m\pi}{n+1}\right)},$$

$$B_m^{(n)} = -\frac{\left(2\cos\frac{m\pi}{n+1} - b\right)\tau}{a - 2\cos\frac{m\pi}{n+1}},$$

$$P_k(x) = -(x+\tau)^k \prod_1^{n-k}{}_j [x - B_j^{(n-k)}].$$

It is easy to show that

$$\lim_{n\to\infty}(-1)^k \frac{A_{n-k}}{A_n} = \frac{1}{\left(1 + \frac{g_1R_s + \sqrt{g_1^2R_s^2 + 4g_1R_s}}{2}\right)^k} = \frac{1}{\alpha^k}, \tag{11}$$

where α is equal to the term in parentheses. Note that if we write $\gamma = R_sg_1$ and let Q be the effective cell spacing, Eq. 10 gives for $t \to 0$ and n large: $V_k(0) = (1/\alpha^k) \cdot V_0(0)$ and hence

$$\lambda = \frac{Q}{\ln\left(1 + \frac{\gamma + \sqrt{\gamma^2 + 4\gamma}}{2}\right)}$$

or

$$\gamma = 2\left(\cosh\frac{Q}{\lambda} - 1\right). \tag{12}$$

Eq. 12 is identical with that obtained by Lamb and Simon (1976, Eq. 14a) in their analysis of the spread of excitation through a purely resistive network.

At all other t we have, for n sufficiently large,

$$V_k(t) = \frac{1}{\alpha^k}\left[V_0(t) - \sum_1^n{}_m \int_0^t {}_kC_m^{(n)}\, e^{B_m^{(n)}(t-\tau)} \cdot V_0(\tau)d\tau\right]. \tag{13}$$

We see, therefore, that initially ($t \to 0$) excitation spreads laterally through the network as though the network contains only resistive elements. The space constant measured early in the response (ideally for $t \to 0$) is determined only by the instantaneous membrane conductance, g_1, and the shunting resistance, according to Eq. 12. We shall call this the instantaneous space constant (λ_{in}) of the network.

It is also useful to define the steady-state value of the length constant (λ_{ss}). This is the space constant measured when relaxation of the time-dependent components of the circuit is complete (ideally for $t \to \infty$). The value of λ_{ss} is defined by Eq. 12 but with $\gamma = R_s(g_1 + g_2)$. A rough idea of the relative magnitudes of g_1 and g_2 can be obtained from the ratio of λ_{in}:λ_{ss}. If $\lambda \gg Q$, $\gamma \approx (Q/\lambda)^2$ and then

$$\frac{g_2}{g_1} = \left(\frac{\lambda_{in}}{\lambda_{ss}}\right)^2 - 1. \tag{14}$$

In 57 cells, the average value of the measured λ_{in} was 24.3 μm and λ_{ss} was 13.1 μm and hence $g_2/g_1 \approx 2.44$.

The solution of Eq. 9 is

$$V_k(t) = \int_0^t \bar{h}_k(t-\tau)\, I_1(\tau)d\tau, \tag{15}$$

where

$$\bar{h}_k(t) = (-1)^k R_s \frac{A_{n-k}}{\bar{A}_n}\left[\delta(t) - \sum_1^n{}_m \bar{C}_m^{(n)}\, e^{\bar{B}_m^{(n)}t}\right],$$

$$\bar{C}_m^{(n)} = \frac{P_k[\bar{B}_m^{(n)}]}{\prod_1^n{}_{m\neq j}[\bar{B}_m^{(n)} - \bar{B}_j^{(n)}]},$$

and

$$\bar{B}_m^{(n)} = \frac{\left[2\cos\frac{(2m-1)}{2n}\pi - b\right]\tau}{\left[a - 2\cos\frac{(2m-1)}{2n}\pi\right]},$$

$$P_k(x) = -(x-\tau)^k \prod_1^{n-k}{}_j [x - B_j^{(n-k)}],$$

$$\bar{A}_n = \prod_1^n{}_m\left[a - 2\cos\left(\frac{2m-1}{2n}\right)\pi\right].$$

In this case it is easily shown that

$$\lim_{n\to\infty}(-1)^k R_s \frac{A_{n-k}}{\bar{A}_n} = \frac{R_s}{(\alpha)^k}\frac{\alpha^2}{(\alpha^2-1)}, \tag{16}$$

where α is defined by Eq. 11. Thus, provided n is sufficiently large, the solution of Eq. 9 is

$$V_k(t) = \frac{R_s}{\alpha^k} \cdot \frac{\alpha^2}{(\alpha^2-1)}\left[I_1(t) - \sum_1^n \int_0^t {}_kC_m^{(n)}\, e^{\bar{B}_m^{(n)}(t-\tau)} \cdot I_1(\tau)d\tau\right]. \tag{17}$$

It is easily seen that the limit of Eq. 16 when $k = 1$ is the input resistance of an infinite resistive cable. Thus, letting $t \to 0$ in Eq. 17 reveals that the system behaves initially as a purely resistive network. This is true when the input is either voltage or current.

The solution of Eq. 9 in the case of an isolated rod ($R_s = \infty$) or in the

case of diffuse illumination is

$$V(t) = \left[\left(1 - \frac{g_1 + g_2}{g_1}\right) e^{-(g_1+g_2/g_1)\tau t} \cdot \int_0^t \frac{\tau}{g_1} e^{(g_1+g_2/g_1)\tau t'} I_1(t')\mathrm{d}t'\right] + \frac{I_1(t)}{g_1}. \quad (18)$$

For the case where $t \to 0$, the ratio of the voltage response elicited by a narrow bar of light at rod 0 to that elicited by diffuse illumination is given by

$$\delta = \frac{V_{\text{bar}}}{V_{\text{diffuse}}} = \frac{R_s g_1 \alpha}{1 - \alpha^2} \quad (19)$$

or with simple algebra

$$\delta = \frac{1}{\sqrt{\left(1 + \frac{4}{\gamma}\right)}}. \quad (20)$$

Note that Eq. 12 allows γ to be expressed in terms of λ and hence Eq. 20 provides a useful test of the theory because the ratio, δ, can be used to calculate λ as a function of time, and this calculated variation can be compared with that measured experimentally using displaced bars of light.

Spread of Excitation: Two-Dimensional Solution

In this treatment we consider a two-dimensional square array of $2n + 1 \times 2n + 1$ rods. Each rod is connected to its four nearest neighbors by a shunting resistance R_s. The electrical properties of the rod membrane are again represented by the transverse circuit element shown in Fig. 2 *a*. The rods are numbered $(1, 1) \ldots (n + 1, n + 1) \ldots (2n + 1, 2n + 1)$ and the same convention is used to define the currents $I_{h,k}$, $j_{h,k}$ and voltages $V_{h,k}$ of the network. We can thus write, for the generalized rod, (h, k),

$$\dot{V}_{h,k} + \frac{(g_1 + g_2)\tau}{g_1} = \frac{\tau}{g_1} I_{h,k} + \frac{\dot{I}_{h,k}}{g_1}. \quad (21)$$

For a square array

$$(I_{h,k}) = (DV + VD - 4V)\frac{1}{R_s} + E, \quad (22)$$

where D, E, V are $2n + 1 \times 2n + 1$ matrices. V is the voltage matrix at each node

$$V = \left\{V_{h,k} \begin{matrix} h = 1 \ldots 2n + 1 \\ k = 1 \ldots 2n + 1 \end{matrix}\right\}.$$

E is the matrix representing the injected extrinsic current

$$E = \{E_{h,k}\},$$

where $E_{h,k}$ is the extrinsic current injected into rod (h, k).

D is a matrix of the form

$$D = \begin{pmatrix} 010 & 0 & & & \\ 101 & & & & \\ 010 & & & & \\ & 010 & & & \\ & 101 & & & \\ 0 & 010 & & & \end{pmatrix}$$

Thus, $(DV + VD)\ (1/R_s)$ is the matrix whose elements represent the current flowing in the rod as a consequence of electrical coupling.

Rearranging Eq. 21 gives

$$A_1\dot{V} + \dot{V}A_1 = A_2V + VA_2 + \frac{\tau E}{g_1} + \frac{\dot{E}}{g_1}, \quad (23)$$

where

$$A_1 = \frac{1}{2}\left(1 + \frac{4}{R_s g_1}\right) I + \frac{1}{R_s g_1} \cdot D$$

and

$$A_2 = -\frac{1}{2}\left[\frac{(g_1 + g_2)\tau}{g_1} + \frac{4\tau}{g_1 R_s}\right] I + \frac{\tau D}{R_s g_1} = \frac{\tau}{g_1 R_s} \cdot \left\{\left[\frac{R_s(g_1 + g_2)}{2} + 2\right] I + D\right\},$$

where I is the $(2n+1) \times (2n+1)$ identity matrix.

Eq. 23 is solved in Appendix B for the case when extrinsic current, $I_0(t)$, is injected at node $n + 1, n + 1$ at the center of the square. In that case, $E_{n+1,n+1} = I_0(t)$ and $E_{h,k} = 0$. The general solution of Eq. 23 is

$$V_{h,k} = \int_0^t f_{h,k}(t - \tau) I_0(\tau)\mathrm{d}\tau, \quad (24)$$

where

$$f_{h,k}(t) = R_s\left\{\sum_1^{2n+1}{}_i \sum_1^{2n+1}{}_j b_{i,j,h,k}\left[\delta(t) + (\tau - Y_{i,j})\right] e^{-Y_{i,j}t}\right\}$$

with

$$b_{i,j,h,k} = \frac{a_{h,i}\, a_{k,j}\, a_{n+1,i}\, a_{n+1,j}}{4 + R_s g_1 + x_i^{(2n+1)} + x_j^{(2n+1)}},$$

$$Y_{i,j} = \frac{\tau[4 + (g_1 + g_2)R_s + x_i^{(2n+1)} + x_j^{(2n+1)}]}{4 + g_1 R_s + x_i^{(2n+1)} + x_j^{(2n+1)}}$$

and

$$a_{i,h} = \frac{(-1)^{i-1} \sin \frac{ih\pi}{2n+2}}{\sqrt{\left(n + \frac{1}{2}\right) - (-1)^h \frac{\sin \frac{(2n+1)}{(2n+2)} h\pi}{2 \sin \frac{h\pi}{2n+2}}}},$$

$$x_j^{(2n+1)} = 2 \cos \frac{j\pi}{(2n+2)}.$$

Eq. 24 is particularly helpful in that it clarifies the relation between the time constants that characterize the responses to various step inputs. If we consider first the case of an isolated rod, $R_s = \infty$, to which a step of voltage is applied (voltage clamp condition), the current will relax with a time constant $\tau_v = 1/Lg_2$. On the other hand, a step of current applied to an isolated rod (current clamp condition) will elicit a voltage that relaxes with a time constant $\tau_c = (g_1 + g_2)/Lg_1g_2$ or $\tau_c = \tau_v\,[(g_1 + g_2)/g_1]$. If we inject a step of current into a coupled network of $(2n+1) \times (2n+1)$ rods, Eq. 24 reveals that the relaxation of the induced voltage will be characterized by $(2n + 1)^2$ time constants, Y_{ij}. It is easy to see that

$$\tau_v < \tau_v\left[\frac{8 + (g_1 + g_2)R_s}{8 + g_2 R_s}\right] < Y_{i,j} < \tau_c. \quad (25)$$

Thus, the time constant of relaxation of voltage elicited by point injection of a DC current step into a coupled network is intermediate between the voltage clamp time constant and the current clamp time constant of an isolated rod.

Eq. 24 also reveals that in the two-dimensional case, as in the one-dimensional case, the excitation in an inductive network of this type spreads initially as in a purely resistive network. For the rod at the center of the array, where h, k is equal to $(n + 1)$, $(n + 1)$, provided n is sufficiently large, the term

$$\sum_{1}^{2n+1}{}_{i} \sum_{1}^{2n+1}{}_{j} b_{i,j,n+1,n+1}$$

is equal to

$$R_{in} = \frac{1}{g_2} \cdot \frac{2}{\pi} \left(\frac{\gamma}{\gamma + 4}\right) K_0 \left[\left(\frac{4}{\gamma + 4}\right)^2\right], \qquad (26)$$

where K_0 is a complete elliptic integral of the first kind. Eq. 26 defines the input resistance of an infinite two-dimensional pure resistive network and is identical with that derived by Lamb and Simon (1976, Eq. 15).

RESULTS

Linearity of the High-Pass Filtering Behavior of the Rod Network

The rod network in the retina of *Bufo marinus* exhibits high-pass filtering behavior closely similar in character to that described in *Chelydra serpentina* by Detwiler et al. (1978, 1980). This is illustrated in Fig. 3 *a*, which shows responses elicited by bar-shaped flashes of monochromatic light (11 μm × 1 mm, wavelength 498 nm), with each flash producing on average 14.06 photoisomerizations (Rh*)/rod. Stimuli were presented at successive 10-μm displacements from the impaled rod. In this case, displacing the stimulus laterally from the centered position (maximal response) to a position 50 μm away caused a decrease in amplitude of the recorded response and a reduction in its time-to-peak from 610 to 450 ms.

The experiment was repeated on the same cell using brighter stimuli that produced on average 28.7 Rh*/rod. The results are shown in Fig. 3 *b*. Note that the centered stimulus elicited a response whose amplitude was greater by a factor of 1.81 than that of Fig. 3 *a*. Displacing the stimulus laterally by 50 μm again caused a reduction in time-to-peak of the record response from 630 to 450 ms.

Each set of responses was used to calculate the electrotonic space constant (λ) as a function of time. The open triangles in Fig. 3 *c* plot the values calculated from the responses of Fig. 3 *a*. The filled circles plot values calculated from the responses of Fig. 3 *b*. Note that in both cases the value of λ falls within 2 s from an initial value of ~30 μm to a steady-state value of ~15 μm. Moreover, the time course of this change is virtually identical in the two cases.

In experiments on 57 rods, the average initial value of λ was 24.3 μm ± 1.1 (SEM), whereas the average steady-state value was 13.1 μm ± 1.0 (SEM). We have been unable to establish whether the spatial decline in the

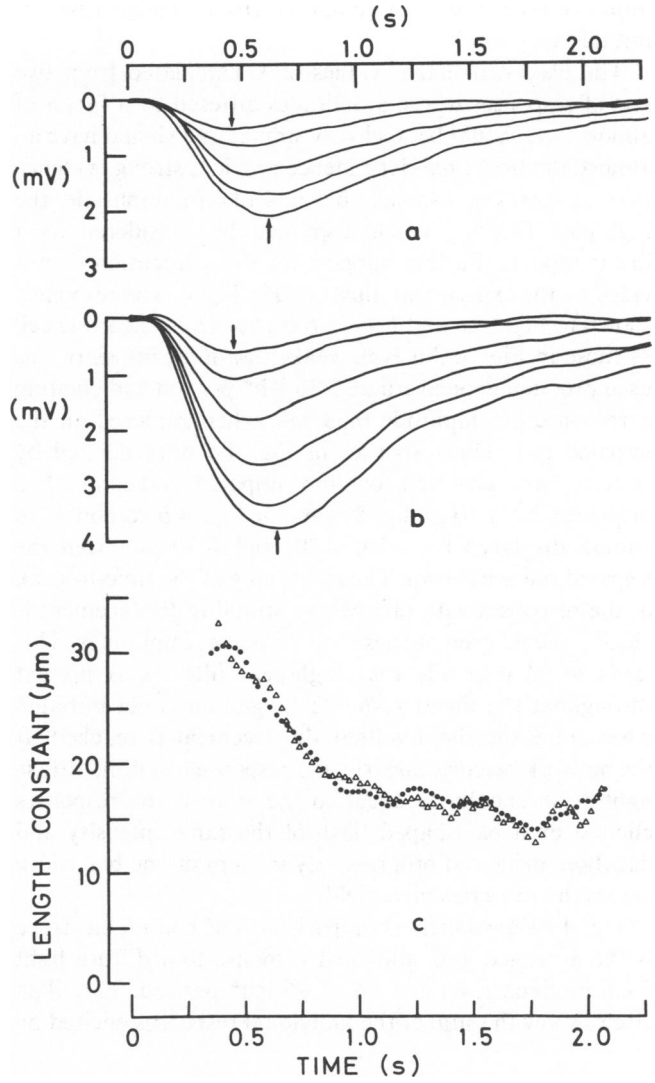

FIGURE 3 The effect of high-pass filtering on voltage responses elicited by stimuli at two different intensities. Slit-shaped stimuli (11 μm × 1 mm) of 50-ms duration and 498-mm wavelength were first centered on the impaled rod and then displaced by successive intervals of 10 μm. Responses in *a* were elicited by stimuli producing 14.06 Rh*/rod. Those in *b* were elicited by stimuli producing 28.7 Rh*/rod. Each trace is the average of eight responses digitally smoothed with $N = 6$ (see Methods). In both cases, displacing the stimulus by 40 μm reduced the time-to-peak of the response from ~610 to ~450 ms. The network length constant calculated from both sets of responses fell from an initial maximum of ~30 to ~15 μm within 2 s as shown in *c*. The open triangles were calculated from the responses shown in *a*, the filled circles from those in *b*.

photovoltage at any given instant is best described by a single exponential or by the sum of several exponentials. The type of plot shown in Fig. 3 *c* should be regarded as no more than a convenient and practical way of illustrating the phenomenon of high-pass filtering by the rod network.

In many experiments, we observed an initial rise in λ early in the response, i.e., within the first 200–400 ms. We have been unable, as yet, to determine whether this effect has a physiological basis or simply represents an uncer-

tainty in the values of λ computed from voltages that are initially very small.

The observation that values of λ, calculated from two sets of responses whose amplitudes differed by a factor of almost two, should be so closely similar and should have an almost identical time-dependence provides strong evidence that, at least for responses below 4 mV in amplitude, the high-pass filtering mechanism can be considered as a linear process. Further support for this contention is provided by the experiment illustrated in Fig. 4. The responses shown in Figs. 4 *a* and *b* were recorded from the same cell as those in Fig. 3. An even weaker stimulus intensity was used producing, on average, 5.86 Rh* per rod and eliciting a response of amplitude 0.93 mV when centered on the impaled rod. The responses in Fig. 4 *a* were elicited by stimuli first centered on the impaled rod and then displaced by +10 and +20 μm. In Fig. 4 *b* responses to stimuli displaced by −10, −20, and −30 μm from the impaled rod are shown. The shortening of the time-to-peak of the responses with progressive stimulus displacement is clearly visible even at these low response amplitudes. This leads us to conclude that high-pass filtering is present throughout the linear response range and is not initiated when some threshold voltage displacement is reached. If the network behaves linearly, the response to a dim, diffuse light flash should be equal to the sum of the responses elicited by a bar-shaped flash of the same intensity and duration, displaced progressively in steps of one bar-width across the rod's receptive field.

Fig. 4 *c* shows such a comparison. The continuous trace is the averaged and smoothed response to a diffuse light flash producing, on average, 5.86 Rh* per rod. The filled circles show the sum of the individual responses elicited by the bar-shaped stimulus at positions 10 μm apart within the range −20 to +20 μm. At locations more distant than 20 μm, the recorded responses were too small to resolve. The agreement is good during the initial part of the response and after ~600 ms. Between 250 and 600 ms, the sum of the individual responses is somewhat smaller than the full-field response. We believe this discrepancy to be due primarily to our failure to record resolvable responses from the more distant parts of the receptive field. Such responses would contribute most strongly in the period over which the discrepancy is greatest. In view of these results, we conclude that the high-pass filtering behavior of the rod network, as manifested in the responses to weak stimuli, can be considered as a linear process and therefore can be analyzed in terms of a linear model.

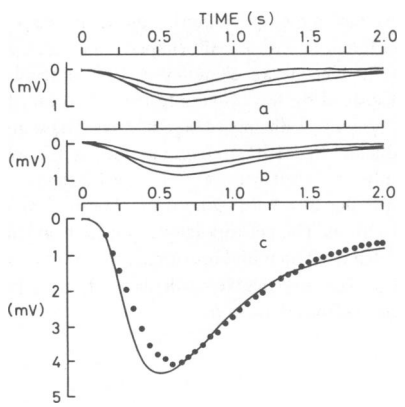

FIGURE 4 A test of the linearity of the network based on the superposition principle. The slit-shaped stimulus centered upon the impaled rod elicited responses of <1 mV (lowest record in both *a* and *b*). Responses were then recorded with the stimulus displaced by 10 and 20 μm on either side (*a* and *b*) of the centered position. A diffuse stimulus of the same intensity elicited the response shown in *c* (continuous wave). The dots represent the sum of the potentials elicited at the five locations tested in *a* and *b*. Each of the continuous curves is the average of twelve recorded responses, smoothed digitally with $N = 6$.

Input Impedance of the Rod Network

Given that the electrical equivalent circuit of the rod membrane in the linear range contains an inductance, we expect to see evidence of its presence in the time course of the voltage change elicited by a step of constant current injected into a rod. Specifically, we expect an initial rapid change in membrane potential to be followed by a slower decay to a steady level that is somewhat closer to the rod's resting potential. To study this behavior, we injected steps of extrinsic, constant current through one barrel of a double-barreled electrode while recording voltage via the second barrel.

Fig. 5 *a* shows the electrode artifact recorded in Ringer's solution for steps of constant current ±0.0225 and ±0.045 nA in amplitude. The coupling resistance in this case was 9.7 MΩ and the time constant of the artifact was <60 ms. Fig. 5 *b* shows the change in membrane potential elicited by steps of extrinsic constant current, ±0.0225 and ±0.045 nA, injected into the rod. These traces were obtained by subtracting the appropriate electrode artifacts (Fig. 5 *a*) from the raw voltage records, using the computer. As shown in Methods, the time course and amplitude of the capacitive transient is independent of both coupling resistance and network input resistance; thus, the time-dependent changes in the elicited voltage, after subtraction of the artifact, must reflect the time-varying properties of the network.

Fig. 5 *c* shows the current-voltage (*I–V*) relation measured 100 ms after initiation of the current steps and in the steady state. The responses to hyperpolarizing and depolarizing current steps of equivalent magnitude were quite symmetrical, which suggests that the membrane voltage changes lay within the linear range. The tails at the cessation of the pulses of ±0.0445 nA were slightly asymmetrical, however. The input resistance 100 ms after initiation of the current step was, in this case, 118 MΩ, relaxing to a steady-state value of 81 MΩ. (Due to limitations of our instrumentation, we were unable to obtain reliable measurements of input impedance within 100 ms of the current step.)

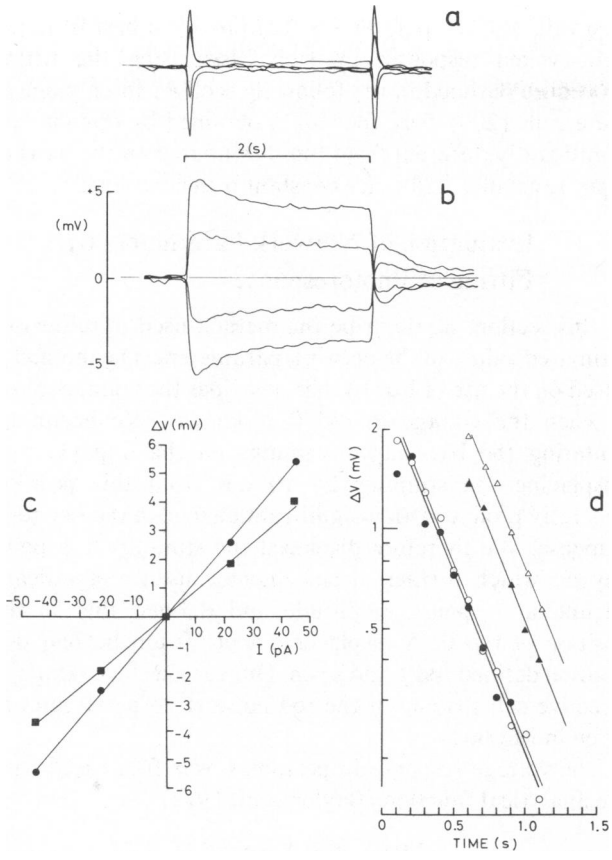

FIGURE 5 The effect of extrinsic current on rod membrane potential. Rectangular pulses of current (±0.0225 and 0.045 nA) of duration 2 s were injected using a double-barreled electrode. (*a*) The artifact resulting from the capacitive coupling of the barrels (transients) and coupling resistance of the electrode (DC voltage displacement), recorded with the electrode tip in Ringer's solution. Each trace is the unsmoothed average of 5 records. (*b*) The change in rod membrane potential evoked by intracellular injection of the same currents. The appropriate capacitive artifact was subtracted digitally from the average of five records to produce each of these traces (see Methods). (*c*) The relation between voltage and injected current measured 100 ms (●) and 1.9 s (■) following onset of the current. (*d*) Time course of the voltage relaxation during and following injection of current. ΔV is the difference between voltage, V_t, at time t and the steady-state voltage, V_∞. Filled and empty circles represent relaxation during injection of +0.045 and −0.045 nA, respectively. Filled and empty triangles represent relaxation of the tail voltages that follow termination of currents +0.045 and −0.045 nA, respectively. For the sake of clarity, these latter data (triangles) have been arbitrarily displaced by +0.5 s.

Fig. 5 *d* shows the relaxation of voltage to the steady state during the current step (circles) and to the resting potential following the cessation of the current (triangles) plotted on log-linear coordinates. The data points for the tail voltages (triangles) have been displaced laterally by +0.5 for clarity. The time constant of relaxation during an outward (depolarizing) step of +0.045 nA (filled circles) was 404 ms, whereas for an equivalent inward (hyperpolarizing) current (open circles) it was 390 ms. Following an outward current step (filled triangles), the tail relaxed with a time constant of 398 ms, whereas after an equivalent inward current step (open triangles) the time constant of relaxation was 400 ms. In all cases, the data were well-fitted by a single time constant. This does not exclude the possibility that the relaxation process might involve additional time constants, however.

Data collected from twenty rods show that 100 ms after onset of the current, the input resistance was 149 ± 20 MΩ (SEM) and this dropped to a steady-state value of 123 ± 14.3 MΩ (SEM) with a relaxation time constant of between 300 and 550 ms.

First Estimate of Circuit Parameters

We can use these data to compute approximate values of network parameters. To do this, we use the analytical result that initially the input resistance and space constant depend only on the values of g_1 and R_s (Eqs. 17 and 26; $t \to 0$). The effective cell spacing of the rod network in *Bufo marinus* is taken to be 10 μm (see Methods). Our collected results give $\lambda_{initial} = 24.3$ μm and $(R_{in})_{100} = 149$ MΩ. These values in turn give $R_s = 364$ MΩ and $g_1 = 0.47 \times 10^{-9}$S.

In the steady state, Eqs. 12 and 26 will apply when $\gamma = (g_1 + g_2)R_s$. Again, from collected data, $\lambda_{ss} = 13.1$ μm and $(R_{in})_{ss} = 123$ MΩ, from which we estimate $R_s \approx 412$ MΩ and $(g_1 + g_2) = 1.48 \times 10^{-9}$S. The two values of R_s differ by <15%, a discrepancy that is within the limits of accuracy of this technique. We take this as support for the view that R_s does not vary with time during small displacements of membrane potential. For the voltage elicited by a step of constant current to relax with a time constant of ~400 ms, L must have a value of $\sim 0.4 \times 10^9$M (Eq. 25).

To summarize, therefore, on the basis of current injections and slit experiments, we estimate the values of the circuit parameters of Fig. 2 *a* to be approximately: $R_s = 388 \cdot 10^6\Omega$ (average of two values), $g_1 = 0.47 \cdot 10^{-9}$S, $g_2 = 1 \cdot 10^{-9}$S, and $L = 0.4 \cdot 10^9$M. We shall refer to these values hereon as our first estimate. Of course, they were obtained from data averaged over many cells.

In the following section, we apply the same procedure to measurements of space constant and input resistance made simultaneously on the same cell in order to test the consistency of the method. Later we will apply Eq. 13 to check that the estimated values of the parameters allow us to reproduce accurately the experimentally observed inductance-like behavior.

Simultaneous Measurement of Unidimensional Space Constant and Input Resistance of the Rod Network

We performed a series of experiments designed to provide, simultaneously, data on the lateral spread of excitation within the network and the network input impedance. An example of such an experiment is shown in Fig. 6. Here, the rod was impaled with a double-barreled electrode and with each displacement of the bar-shaped light stimulus,

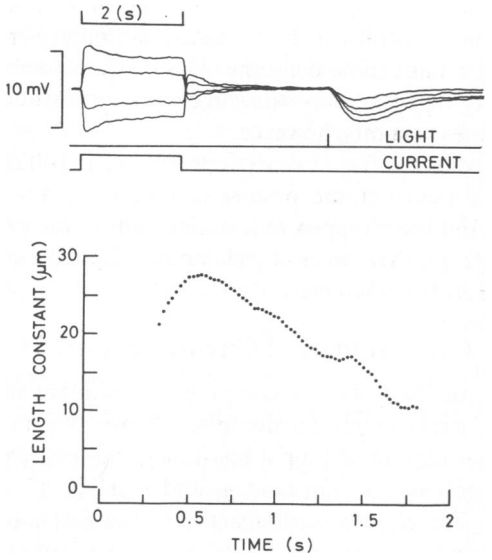

FIGURE 6 Simultaneous measurement of network length constant and input impedance. The traces in the upper panel show current-evoked potential changes followed by voltage responses elicited by the slit-shaped stimulus at 10-μm intervals between the centered position and a lateral displacement of 30 μm (each trace the average of five responses, $N = 0$). The length constant of the network, calculated as a function of time from the light-evoked responses, is plotted in the lower panel. (Same cell as Fig. 5.)

the amplitude of the injected current step was also changed. The traces in the upper panel of Fig. 6 clearly show the pronounced relaxation of voltage during injection of the current step and the shortening of the time-to-peak of the light-evoked response as the stimulus was displaced. In the lower panel of Fig. 6, the network length constant, calculated from the light-evoked responses shown above, is plotted as a function of time. The current-voltage relation for this cell and the time constant of voltage relaxation are those shown in Fig. 5.

The collected data from five successful experiments of this type are presented in Table I. The values of R_s, g_1, and of $(g_1 + g_2)$ were calculated from these data using the same procedure as before. The last four columns of Table I give values of the parameters that provide a best fit to the light-evoked responses in each case, using the fitting procedure outlined in the following section. In only one of these cells (203) were the values obtained by this method significantly different from those estimated on the basis of input resistance and space constant measurements.

Evaluation of Network Parameters by Fitting of Photoresponses

In this section, we describe the method used to refine our estimated values of the network parameters. The method is based on the use of Eq. 10 that describes the voltage in rod k when the voltage in rod 0 is known. We began by centering the bar-shaped stimulus on the impaled rod. Displacing the stimulus by 10 μm from this position generally produced an insignificant change in the recorded response. We therefore displaced the stimulus to a point beyond which further displacement caused a significant decline in response amplitude and defined this as the position of rod 0. A displacement of 10 μm beyond this position defined rod 1 and so on. Our reasons for taking the effective cell spacing of the rod network to be 10 μm are given in Methods.

The voltage response in position 0 was first fitted with the analytical function (Baylor et al. 1974)

$$V(t) = A(e^{-\alpha t} - e^{-\beta t})^n, \qquad (27)$$

where A is a scaling factor, α and β are time constants, and n is an integer. This yields a simple analytical expression that can be used in solving Eq. 10. A good fit was obtained with $n = 4$, although $n = 3$ also provided a satisfactory approximation in most cases. The value of α lay in the range 0.15 to 0.55 s^{-1}, whereas β ranged between 1.6 and 5.3 s^{-1} in 26 different cells. By fitting the theoretically generated voltages to the experimentally recorded responses of rods 1, 2, 3, . . . etc., the parameters g_1, g_2, L, and R_s could be evaluated. Fitting was achieved using a minimizing routine kindly provided by Dr. Dennis Pelli of the University of Cambridge. The initial values of the parameters were those of our first estimate; R_s = 388 ·

TABLE I
SIMULTANEOUS MEASUREMENT OF λ AND R_{in}: COLLECTED DATA FROM FIVE EXPERIMENTS

Cell	A				B				C			
	$R_{in}(100)$	λ_{in}	R_s	g_1	$R_{in}(ss)$	λ_f	R_s	$g_1 + g_2$	g_1	g_2	R_s	L
	MΩ	*μm*	*MΩ*	*10^{-9}S*	*MΩ*	*μm*	*MΩ*	*10^{-9}S*	*10^{-9}S*	*10^{-9}S*	*MΩ*	*10^9M*
200–2	117	27	274	0.5	84	12	298	2.47	0.5	2	286	0.2
200–4	133	30	277	0.26	133	30	277	0.26	0.26	—	277	—
201	100	32	219	0.45	87	27	204	0.68	0.45	0.23	210	1.5
202	145	34	313	0.28	126	15	389	1.18	0.1	1.08	270	0.5
203	128	40	260	0.24	108	20	288	0.88	0.1	1.2	100	0.4

(A) $R_{in}(100)$, input resistance at 100 ms; λ_{in}, initial length constant; R_s and g_1 obtained from Eqs. 12 and 26 with D = 10 μm. (B) $R_{in}(ss)$, steady-state input resistance; λ_f, final length constant; R_s and $(g_1 + g_2)$ obtained from Eqs. 12 and 26 with D = 10 μm and measured values of $R_{in}(ss)$ and λ_f. (C) g_1, g_2, R_2, and L are values of these parameters obtained by fitting the response waveforms using routine FITSLI.

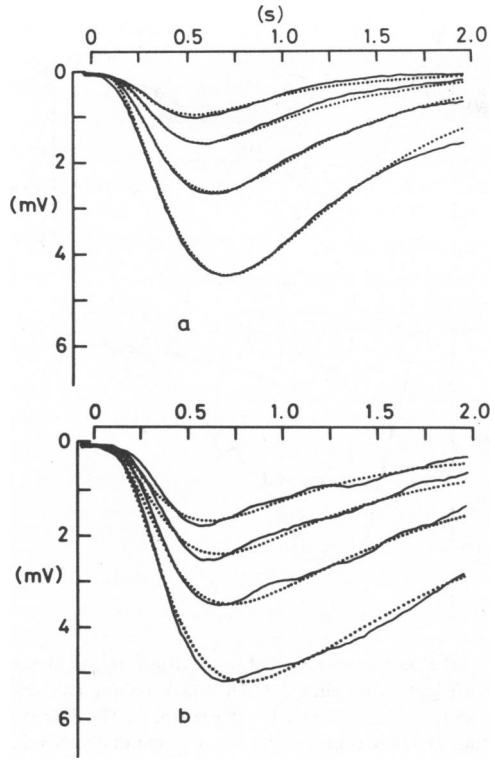

FIGURE 7 Responses recorded in two different rods, elicited by slit-shaped stimuli at displacements of 0, 10, 20, and 30 μm (continuous traces). Each trace is the smoothed ($N = 6$) average of six responses. The dotted curves are theoretical responses predicted by the model using the following values of the network parameters: (*a*) $R_s = 270$ MΩ, $g_1 = 0.311 \cdot 10^{-9}$S, $g_2 = 1.19 \cdot 10^{-9}$S, and $L = 0.28 \cdot 10^9$H; (*b*) $R_2 = 300$ MΩ, $g_1 = 0.2 \cdot 10^{-9}$S, $g_2 = 0.8 \cdot 10^{-9}$S, and $L = 1.10^9$H. See text for full details of the fitting procedure.

$10^6\Omega$, $g_1 = 0.47 \cdot 10^{-9}$S, $g_2 = 1 \cdot 10^{-9}$S, and $L = 0.4 \cdot 10^9$H. The program terminated when a minimum was found. Checks were made to ensure that other local minima were not present.

Fig. 7 *a* shows our most successful application of this procedure. A more typical example is shown in Fig. 7 *b*. The dotted lines plot the theoretical curves generated by Eq. 10. The solid lines are the experimental records. Note that only in the case of rod 0, the centered position, was the theoretical curve scaled to fit the experimental response.

The fitting was reasonably successful in all of the 26 cells analyzed. A systematic discrepancy was observed in the fitting of the responses between 150 and 400 ms at the more distant positions. This is clearly seen in Fig. 7 *b*. As noted earlier (e.g., Fig. 6), the length constant during this interval generally increases to its maximum value before declining to its steady-state value. This cannot be accounted for by any of the models shown in Fig. 2 and suggests that the equivalent circuit of the rod membrane contains a capacitance that has a significant effect early in the response. The average values of the parameters obtained from 26 cells using this procedure were: $g_1 = 0.26 \pm 0.03 \times 10^{-9}$S, $g_2 = 0.88 \pm 0.08 \times 10^{-9}$S, $R_s = 310 \pm 24$ MΩ, and $L = 0.74 \pm 0.1 \times 10^9$M. This evaluation of the network parameters is slightly different from our earlier estimate, though not greatly so. The differences, we believe, are due to our inability to obtain a true initial value of the network length constant ($t \approx 0$) upon which the earlier estimates were heavily dependent. It is also likely that the input resistance 5–10 ms after onset of the current step was in reality higher than that which we measured after 100 ms. The values of parameters given above will be referred to as our standard values and used throughout the remainder of the analysis.

Time Course and Sensitivity of Responses to Bar-shaped and Diffuse Stimuli

A consequence of high-pass filtering by the rod network is that the time course of the response to diffuse illumination is faster than that of the response to a centered bar-shaped stimulus. This is clearly seen in the records of Fig. 4; the response to the diffuse stimulus peaks some 150 ms earlier than that elicited by the bar.

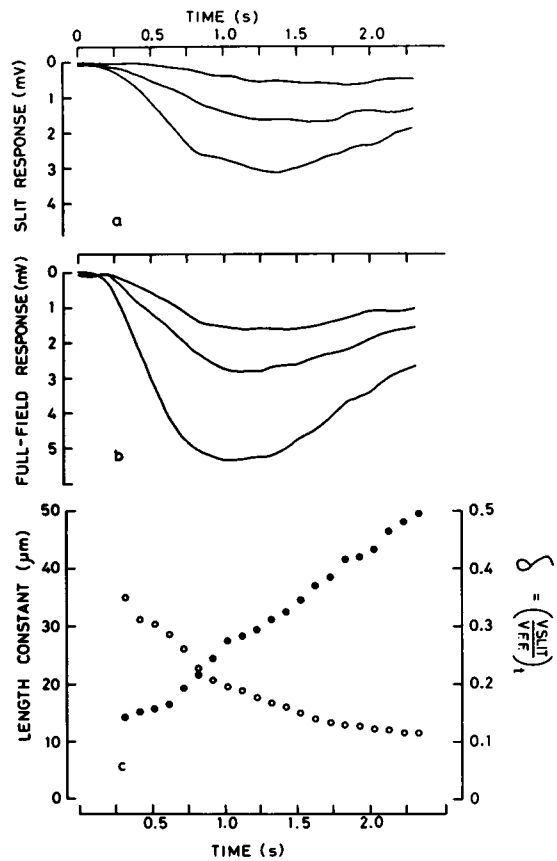

FIGURE 8 (*a*) Responses elicited by the slit-shaped stimulus, centered on the impaled rod, at three different intensities that produced on average 1.3, 3.1, and 5.8 Rh*/flash. (*b*) Responses elicited from the same rod by diffuse stimuli of the same intensities. (*c*) The ratio δ is plotted as a function of time during the response (filled circles). The length constant of the network, calculated from the values of δ, as a function of time during the response is plotted by the open circles.

In Fig. 8 *a*, voltage responses elicited by centered bar-shaped stimuli of three different intensities are presented. In Fig. 8 *b*, responses elicited by diffuse stimuli of the same three intensities are presented. The intensities produced on average 1.3 Rh*/flash, 3.1 Rh*/flash, and 5.8 Rh*/flash, respectively.

It is clear from Figs. 8 *a* and *b* that when the bar-shaped stimulus is used, the linear response range extends perhaps to 2 mV, whereas under diffuse illumination it may extend up to 3–4 mV. From these and other data we determined that, in this rod, a stimulus of either configuration elicited a linear range response provided stimulus intensity was not much greater than 3.1 Rh*/flash.

In Fig. 8 *c* we have plotted as a function of time (filled circles) the ratio of the photovoltage elicited by the bar-shaped stimulus to that elicited by diffuse illumination of the same intensity (3.1 Rh*/flash). This ratio, δ, slowly increases from an initial value of ~0.15 to a final value near 0.5. This implies that the sensitivity of the rod to the bar-shaped stimulus is initially 6–7 times less than to diffuse illumination, but near the end of the response, it is only 2 times less than to diffuse illumination.

These data provide us with a useful test of the theory. From Eq. 20, knowing δ we can obtain γ. Knowing γ as a function of time and using Eq. 12, we can calculate the change in network length constant (λ) as a function of time. Following this procedure, and taking D to be 10 μm (Methods), we calculated the variation in λ with time, which is plotted as the open circles in Fig. 8 *c*. Note that the calculated length constant falls from an initial value of ~30 to ~12 μm over an interval of 2 s. This is in good agreement with the variation in λ measured experimentally (see Figs. 3 and 6, for example), an agreement that argues for the internal consistency of the theory.

Photovoltage and Photocurrent

In the linear response range, when full-field illumination is used (<~3 Rh*/flash), the relation between photocurrent and photovoltage is

$$Lg_2\dot{I} + I = Lg_1g_2\dot{V} + (g_1 + g_2)V. \qquad (28)$$

Eq. 28 can be used to obtain the photovoltage when the photocurrent is known, or to obtain the photocurrent when the photovoltage is known. In the latter case, we obtain

$$I(t) = \frac{1}{L}\int_0^t e^{-(t-t')/Lg_2}\,V(t')\mathrm{d}t' + g_1V(t). \qquad (29)$$

In Fig. 9 we show the result of this procedure. In Fig. 9 *a* the continuous line plots the response to a diffuse light of intensity equivalent to 1.3 Rh*/flash. This is the same cell as used in Fig. 8. The dotted line was obtained by fitting the analytical function (Eq. 27) to the measured response. The best fit was obtained with $n = 4$, $\alpha = 0.2385$, and $\beta = 1.895$. Substituting the standard values given earlier in Eq. 29, we obtain the broken line which represents the time

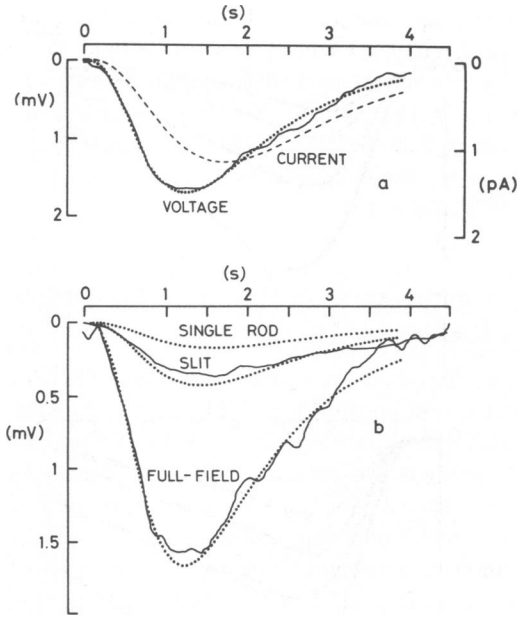

FIGURE 9 (*a*) Rod response elicited by a diffuse (full-field) stimulus of intensity sufficient to produce 1.3 Rh*/flash (continuous trace). The dotted line represents Eq. 27 fitted to this response. The dashed line plots the magnitude and time course of the photocurrent that yields this voltage response as calculated using the network model (details in text). (*b*) Rod responses elicited by a diffuse stimulus and by a centered slit-shaped stimulus of equal intensity (continuous traces). The dotted lines represent the responses predicted by the network model (using the standard parametric values $R_s = 310$ MΩ, $g_1 = 0.26 \cdot 10^{-9}$S, $g_2 = 0.88 \cdot 10^{-9}$S, and $L = 0.74 \cdot 10^9$ H for the case of a diffuse stimulus, slit-shaped stimulus, and illumination of the impaled rod only, for a photocurrent having the time course shown in *a*.

course of the photocurrent. The peak value of the current is 1.16 pA in this case, which yields a quantal photocurrent of ~0.9 pA per photoisomerization.

As a further check of the internal consistency of our theoretical treatment, we next used the calculated photocurrent to compute the voltage response of the rod to diffuse illumination, to a centered bar-shaped stimulus and to illumination restricted to the impaled rod. To do this, we first approximated the calculated photocurrent by the analytical function

$$I(t) = B(e^{-\alpha t} - e^{-\beta t})^n. \qquad (30)$$

The similarity to Eq. 27 is obvious. A best fit was obtained with $n = 4$, $\alpha = 0.1955$, $\beta = 1.31833$, and B adjusted to give a peak photocurrent of 1.16 pA. This function was then applied to Eqs. 18, 15, and 24, respectively. The results are presented in Fig. 9 *b*.

The time courses of the voltage responses, predicted by the model using the standard values of the network parameters for the three different stimulus configurations, are given by the dotted curves. The continuous lines plot responses to diffuse illumination and to the centered bar-shaped stimulus recorded from the same rod as was used for Fig. 8. The agreement is satisfactory. The

different voltage time courses elicited by the three different classes of stimulus are clearly seen. Note that initially the sensitivity of the rod to diffuse illumination is ~7 times greater than to the centered, bar-shaped stimulus and ~23 times greater than to single cell illumination. Three to four seconds later, these sensitivities are in the ratio ~2.5 and ~5.4, respectively.

Consequences of High-Pass Filtering by the Rod Network

So far, we have been primarily concerned with the shortening in the time-to-time peak of the voltage response as it propagates laterally through the network. The model satisfactorily predicts this behavior as can be seen in Fig. 10. The traces shown in Fig. 10 *a* were generated by the unidimensional model (Eq. 15), using the standard values of the network parameters and the theoretical photocurrent shown in Fig. 9 *a*. They describe the voltage responses that would be elicited in rods 1, 2, . . . 7, respectively, by a dim bar-shaped flash of light centered on rod 0. Note that the time-to-peak of the response shortens from 1.45 s in rod 1 to 1.0 s in rod 7.

Fig. 10 *b* shows similar results, this time generated by the two-dimensional model (Eq. 24), but using the same

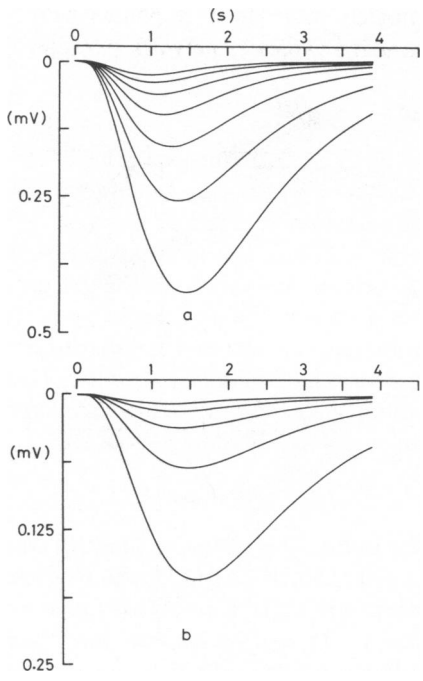

FIGURE 10 Voltage responses to laterally displaced stimuli, predicted by the one-dimensional and two-dimensional network models, when the input is the theoretical photocurrent shown in Fig. 9*a*. (*a*) Prediction of the one-dimensional model for stimulation by a narrow slit of light at successive 10-μm displacements from the impaled rod. (*b*) Prediction of the two-dimensional model for stimulation of single rods at successive 10-μm displacements from the impaled rod. R_s = 310 MΩ, $g_1 = 0.26 \cdot 10^{-9}$S, $g_2 = 0.88 \cdot 10^{-9}$S, and $L = 0.74 \cdot 10^{9}$H.

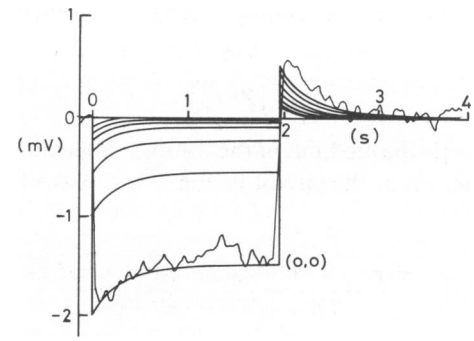

FIGURE 11 Voltage displacements that would be recorded in rod (0, 0) during injection of rectangular current pulses of −0.0137 nA into rods (0, 0) → (0, 6), respectively, calculated using the two-dimensional network model. The voltage displacement, recorded experimentally during injection of this current into the impaled rod (0, 0), is shown for comparison.

network parameters and theoretical photocurrent. The traces thus describe the voltage responses that would be elicited in rods (0, 0), (0, 1), (0, 2), (0, 3), and (0, 4) by a weak flash of light on rod (0, 0) only. In this case, the time-to-peak of the response falls from 1.6 s in (0, 0) to 1.2 s in (0, 4).

Because the theoretical photocurrent used to generate Fig. 10 was computed from responses elicited by a stimulus equivalent to 1.3 Rh*/flash, Fig. 10 *b* represents, to a close approximation, the spread of excitation through the rod network following the absorption of a single photon by a single rod. The model predicts that the response elicited by a single photon is 174 μV in the stimulated rod and only 9 μV in a rod 40 μm away.

In Fig. 11 we see the voltage changes in rods (0, 0), (0, 1), . . . (0, 6) predicted by the two-dimensional model for the case of a −0.0137 nA step of current injected into rod (0, 0). For comparison we show the experimentally measured voltage recorded in rod (0, 0) during injection of a current step of this magnitude using a double-barreled electrode. It is not meaningful to compare time courses within 30–50 ms of current onset or offset because the model takes no account of membrane capacitance and because this is where any error in subtracting the capacitive electrode artifact is likely to be maximal. Over the remainder of the time course, however, agreement is satisfactory.

The theoretically generated curves show clearly that it is primarily the transient components of the signal that are transmitted to the more distant rods, a result earlier demonstrated in the rod network of the tiger salamander by Attwell and Wilson (1980). Thus, the length constant of the network is higher for the high frequency components of the signal than for the low frequency components. This is consistent with the fall in length constant as a function of time that we observed earlier in the responses to luminous stimuli.

The frequency dependence of the network length con-

stant can be calculated, simply, from Eq. 12, where

$$\gamma = \frac{R_s}{|Z(f)|} \tag{31}$$

and $|Z(f)|$ is the modulus of the complex impedance of the membrane. From the circuit of Fig. 3 *a* it is easily shown that

$$|Z(f)| = \frac{\sqrt{[g_1 + g_2 + (2\pi f L g_2)^2 g_1]^2 + (2\pi f L g_2^2)^2}}{(g_1 + g_2)^2 + (2\pi f L g_1 g_2)^2}. \tag{32}$$

In Fig. 12 *a* are plotted $|Z(f)|$ and network length constant (λ) as functions of frequency. Note that the frequency characteristics of the membrane are reflected almost exactly in the frequency characteristics of the network length constant. In Fig. 12 *b*, for comparison, we have plotted the normalized frequency characteristics of the theoretical photocurrent; i.e.,

$$|A(f)| = |F[(e^{-\alpha t} - e^{-\beta t})^n]|, \tag{33}$$

where $F[]$ indicates the Fourier transform of a function. Eq. 33 was computed analytically.

From Fig. 12 *a* it is clear that signals with component frequencies between 0 and 0.1 Hz or between 10 and ∞ Hz will be propagated with no significant distortion. It is also clear from Fig. 12 *b*, however, that the photocurrent contains component frequencies in the range 0.1 and 1 Hz and thus we would expect photovoltages to be propagated with some distortion as, indeed, we observe.

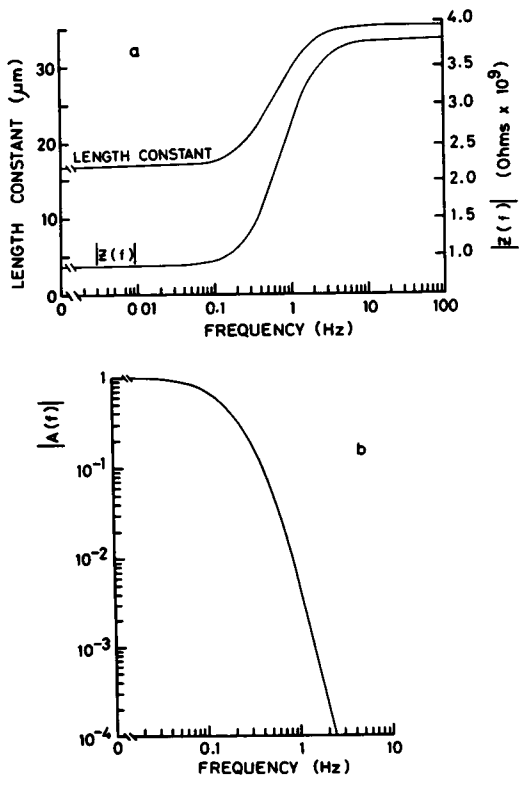

FIGURE 12 (*a*) The network length constant and the absolute value of the complex impedance of the rod membrane, calculated using the standard network parameters, are plotted as functions of frequency of the stimulus. (*b*) The normalized frequency spectrum of the theoretical photocurrent, calculated as described in the text.

Dependence of Voltage Response Time Course on Parametric Values

In any quantitative study of the ionic properties of the rod membrane (see following paper) it is important that the effects of changing individual values of network parameters be properly understood. In this section, the effects of such changes upon the high-pass filtering properties of the network will be discussed.

Changes in R_s. The high-pass filtering property is not dependent upon R_s. This is clearly seen in Eq. 13 *b*, where the ratio $\lambda_{in}/\lambda_{ss}$ is independent of R_s. Of course the absolute values of both λ_{in} and λ_{ss} are similarly dependent upon R_s (Eq. 12). Changes in R_s are equivalent to appropriate changes in the effective cell spacing, *D*.

Changes in g_2. The obvious way in which the high-pass filtering property can be suppressed is to reduce or eliminate the current flowing through the arm of the circuit containing the inductance; i.e., to decrease g_2. In Fig. 13 *a* are the responses, predicted by the model, to narrow bars of light at successive 10-μm displacements from the impaled rod. These responses were generated using the standard values of network parameters and the

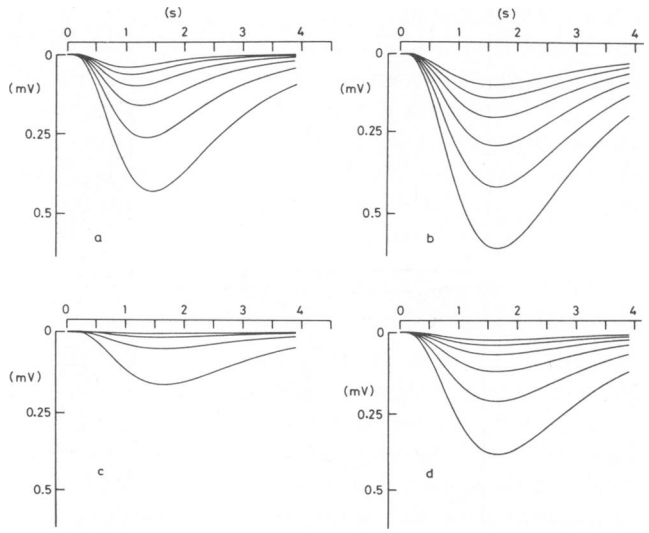

FIGURE 13 The effect upon high-pass filtering by the rod network of a change in the value of one of the network parameters. In each panel, computer simulated responses to a slit-shaped stimulus at successive 10-μm displacements between 0 and 50 μm are presented. (*a*) Responses computed with the standard parameter values. R_s = 310 MΩ, $g_1 = 0.26 \cdot 10^{-9}$S, $g_2 = 0.88 \cdot 10^{-9}$S; $L = 0.74 \cdot 10^9$H. (*b*) The effect of reducing g_2 by a factor of 4. ($g_2 = 0.22 \cdot 10^{-9}$S) (*c*) The effect of increasing g_1 by a factor of 16. ($g_1 = 4.16 \cdot 10^{-9}$S) (*d*) The effect of reducing *L* by a factor of ~8. ($L = 0.092 \cdot 10^9$H).

theoretical photocurrent plotted in Fig. 8 *a*. In fig. 13 *b*, we show the effect of reducing g_2 to one quarter of its standard value, i.e., from $0.88 \cdot 10^{-9}$S to $0.22 \cdot 10^{-9}$S. The peak amplitude of the response at each stimulus position is increased by ~40% and the time-to-peak of the response to a centered stimulus is also increased. More importantly, the shortening in the time-to-peak with stimulus displacement is greatly reduced, indicating almost complete elimination of the high-pass filtering by the network. In this case, the length constant, λ, remains virtually constant at its initial (highest) value. A less than fourfold reduction in g_2 reduces but does not eliminate the high-pass filtering behavior of the network.

Changes in g_1. The high-pass filtering by the network will also be reduced if the fraction of current flowing through the purely resistive arm of the circuit is increased. Increasing the value of g_1 will accomplish this and also, as is evident in Eq. 13 *b*, will decrease the initial value of the network length constant and decrease the difference between initial and steady-state values of the length constant. This is illustrated in Fig. 13 *c*. A 10–16-fold increase in g_1 is necessary to reduce the high-pass filtering behavior to a negligible level.

Changes in L. The dependence of the high-pass filtering behavior on the value of L is critically dependent upon the frequency content of the input signal. From Eq. 32 is it clear that a decrease in the value of L is equivalent to a shift of $|Z(f)|$ and $\lambda(f)$ towards higher frequencies. Thus, if L is increased sufficiently to allow almost all of the frequencies contained in the input signal to be transmitted laterally with the low-frequency value of λ, the signal will be propagated with minimal distortion. In other words, the signal frequencies will lie below the band pass of the high-pass filter. As shown in Fig. 13 *d*, a roughly eightfold decrease in L is necessary for this to occur. In this case, the length constant will assume the steady-state (low) value.

DISCUSSION

The spread of linear-range excitation through the rod network in the retina of the toad, *Bufo marinus*, is satisfactorily described by the circuit shown in Fig. 2 *a*. This agrees with the conclusions of Detwiler et al. (1980), who used the same circuit to fit responses of rods in the turtle retina. It should be remembered, however, that the circuits shown in Figs. 2 *b* and *c* yield equivalent equations and thus should not be regarded as being any less valid as possible models of the network.

Our treatment yields one consistent discrepancy as was pointed out earlier. The theory does not provide an accurate prediction of the response time course during the interval between 150 and 400 ms following stimulation. The discrepancy is greater with larger displacements of the bar-shaped stimulus. This is consistent with the early increase in λ during this interval that we have observed in most of the rods studied (see Fig. 6 of this paper and Fig. 2 of the following paper for typical examples). We believe that this discrepancy may be due to the presence of a capacitance in the equivalent circuit of the rod membrane, which we have not considered in our present analysis.

Of course, the simple, regular, one- and two-dimensional networks we have analyzed are only rough approximations to the true rod network of the toad retina. Histological cross sections reveal a rather more irregular distribution of rods than the model would suggest. This factor should not invalidate the qualitative conclusions drawn on the basis of the model, though it must lend a small degree of uncertainty to the absolute values of parameters deduced from the fitting procedures we have used. Further, and perhaps more significant, errors may have resulted from the effects of light scatter and of residual electrode artifacts. Nonetheless, the consistency of the various estimates of network parameters and the intrinsic consistency of the model suggests that the estimated values should not be greatly in error.

The theoretical photocurrent shown in Fig. 9 *a* and subsequently used in estimating the quantal photocurrent of the rod was computed from voltage responses of one of the more sensitive rods from which we recorded. It had a flash sensitivity of 2.3 mV/Rh*, compared with an average value of 1 mV/Rh*, and the time course of its response was also marginally slower than usual. It is likely, therefore, that a more typical value of the peak photocurrent elicited by 1 Rh* is near 0.4 pA with a time-to-peak of 1–1.3 s.

Lamb et al. (1981) found that in Ringer's solution buffered with bicarbonate and 5% CO_2, toad rods are roughly one-fourth as sensitive as had been previously measured in HEPES-buffered Ringer's solution (Baylor et al., 1979): 1 Rh* yielding a photocurrent of ~0.25 pA. Thus our estimation of quantal photocurrent is in satisfactory agreement with their value, measured under equivalent experimental conditions. Having analyzed a circuit model of the rod network in the toad retina and established reliable values for the circuit parameters, we can now use it to determine the identity of the ionic mechanism responsible for the high-pass filtering behavior. This is described in the following paper.

We wish to thank Professor Sir Alan Hodgkin for numerous helpful discussions throughout the course of this work and for suggesting model 3 of our analysis. We are grateful, too, to Dr. P. A. McNaughton, Dr. T. D. Lamb, Dr. K.-W. Yau, and Dr. D. Pelli for their suggestions and comments, and to Mr. R. H. Cook for his excellent technical assistance.

This work was supported in part by grants from the Medical Research Council of Great Britain (to Professor Hodgkin), the National Eye Institute (EY00113 and EY02493 to W. G. Owen), and European Molecular Biology Organization fellowship (to V. Torre).

Received for publication 22 June 1982 and in final form 24 September 1982.

APPENDIX A

In this appendix we give in detail the solution of (*a*) Eq. 8 and (*b*) Eq. 9.

(*a*) The equation to be solved is

$$A\dot{V} = -\tau BV - C, \tag{A1}$$

where A, V, B, C, and τ are as defined in the text. The system of equations represented by Eq. A1 can be solved using Laplace methods. Let

$$\begin{aligned} V(s) &= L[V(t)] \\ C(s) &= L[C(t)], \end{aligned} \tag{A2}$$

where L represents the Laplace transform of a function. Eq. (A1) becomes

$$A[sV(s) - V(0)] = -\tau BV(s) - C(s). \tag{A3}$$

Using the initial condition $V(0) = 0$, this simplifies to

$$(sA + \tau B)V(s) = -C(s) \tag{A4}$$

or

$$(s + \tau)GV(s) = -C(s), \tag{A5}$$

where

$$G = \begin{pmatrix} c10 & 0 & & \\ 1c1 & & & \\ 01c & & & \\ & c10 & & \\ & 1c1 & & \\ 0 & 01c & & \end{pmatrix}$$

and $c = (sa + \tau b)/(s + \tau)$. Thus,

$$V(s) = -\frac{G^{-1}}{s + \tau} C(s). \tag{A6}$$

The inversion of a matrix of the form G is described in Appendix D. This yields

$$V(s) = \frac{-(-1)^{k+1}}{s + \tau} \cdot \frac{S_{n-k}(c)}{S_n(c)} \cdot (s + \tau)\, V_0(s), \tag{A7}$$

where $S_n(x)$, as specified in Appendix D, is a Chebyshev polynomial of the second type of order n. The inverse transform of Eq. A7 will give the solution in the time domain. The zeroes of $S_n(x)$ are given in theorem 22.16.5 (Abramowitz and Stegun, 1964), and they are both real and simple; i.e.,

$$S_n(x) = \prod_1^n{}_m (x - x_m^{(n)}),\ x_m^{(n)} = 2\cos\frac{m\pi}{n+1}. \tag{A8}$$

Eq. A7 can thus be rewritten as follows

$$\begin{aligned} V_k(s) &= (-1)^k \frac{S_{n-k}(c)}{S_n(c)} V_0(s) \\ &= (-1)^k \frac{\prod_1^{n-k}{}_j [c - x_j^{(n-k)}]}{\prod_1^n{}_m [c - x_m^{(n)}]} V_0(s) \\ &= (-1)^k (s + \tau)^k \\ &\quad \cdot \frac{\prod_1^{n-k}{}_j \{s[a - x_j^{(n-k)}] + \tau[b - x_j^{(n-k)}]\} V_0(s)}{\prod_1^n{}_m \{s[a - x_m^{(n)}] + \tau[b - x_m^{(n)}]\}} \end{aligned}$$

or

$$V_k(s) = (-1)^k (s + \tau)^k \frac{\prod_1^{n-k}{}_j [a - x_j^{(n-k)}]}{\prod_1^n{}_m [a - x_m^{(n)}]} \cdot \frac{\prod_1^{n-k}{}_j \left\{ s + \frac{\tau[b - x_j^{(n-k)}]}{[a - x_j^{(n-k)}]} \right\}}{\prod_1^n{}_m \left\{ s + \frac{\tau[b - x_m^{(n)}]}{[a - x_m^{(n)}]} \right\}} V_0(s). \tag{A9}$$

Hence, the Laplace transform of the impulse response, $h_k(t)$ is

$$H(s) = (-1)^k (s + \tau)^k \cdot \frac{\prod_1^{n-k}{}_j [a - x_j^{(h-k)}]}{\prod_1^n{}_m [a - x_m^{(n)}]} \cdot \frac{\prod_1^{n-k}{}_j [s - B_j^{(n-k)}]}{\prod_1^n{}_m [s - B_m^{(n)}]}. \tag{A10}$$

This can be inverted using standard inverse transform formulas to give

$$h_k(t) = (-1)^k \frac{\prod_1^{n-k}{}_j [a - x_j^{(n-k)}]}{\prod_1^n{}_m [a - x_m^{(n)}]} \cdot \left\{ \delta(t) - \sum_1^n \frac{P_k[B_m^{(n)}]\, e^{B_m^{(n)} t}}{\prod_{1 \neq m}^n{}_j [B_m^{(n)} - B_j^{(n)}]} \right\}, \tag{A11}$$

where $B_m^{(n)}$ and $P(x)$ are as defined in the text.

(*b*) In this case, the equation to be solved is

$$\bar{A}\dot{V} = -\tau\bar{B}\dot{V} - \bar{C}, \tag{A12}$$

where $\bar{A}$, $\bar{B}$, $\bar{C}$, V, and τ are as defined in the text. The method of solution of this equation is similar to that used in solving Eq. A1. Again, taking the Laplace transform gives

$$(s\bar{A} + \tau\bar{B})\, V(s) = -\bar{C}(s) \tag{A13}$$

or

$$(s + \tau)\, \bar{G}V(s) = -\bar{C}(s), \tag{A14}$$

where $\bar{G}$ has the form

$$\bar{G} = \begin{pmatrix} c200 & 0 & & \\ 1c10 & & & \\ 01c1 & & & \\ 001c & & & \\ & & 1c1 & \\ 0 & & 01c & \end{pmatrix}$$

and

$$c = \frac{as + \tau b}{(s + \tau)}. \tag{A15}$$

Inverting the matrix, $\bar{G}$, by the method described in Appendix D yields

$$V_k(s) = -\frac{R_s(-1)^{k+1}}{s+\tau}\frac{S_{n-k}(c)}{C_n(c)} J_1(s)(s+\tau), \tag{A16}$$

where $C_n(x)$ is also a Chebyshev polynomial as specified in Appendix D and $J_1(s)$ is the Laplace transform of $I_1(t)$. The zeroes of $C_n(x)$ are given in theorem 22.16.4 (Abramowitz and Stegun, 1964), and are again real and simple.

$$C_n(x) = \prod_1^n{}_m [x - y_m^{(n)}]; y_m^{(n)} = 2\cos\frac{2m-1}{2n}\cdot\pi. \tag{A17}$$

Eq. A16 thus becomes

$$V_k(s) = R_s(-1)^k \frac{S_{n-k}(c)}{C_n(c)} J_1(s).$$

By similar logic to that used earlier, this can be written

$$V_k(s) = (-1)^k(s+\tau)^k \cdot \frac{\prod_1^{n-k}{}_j[a - x_j^{(n-k)}] \prod_1^{n-k}{}_j\left\{s + \frac{\tau[b - x_j^{(n-k)}]}{[a - x_j^{(n-k)}]}\right\}}{\prod_1^n{}_m [a - y_m^{(n)}] \prod_1^n{}_m\left\{s + \frac{\tau[b - y_m^{(n)}]}{[a - y_m^{(n)}]}\right\}} \cdot J_1(s). \tag{A18}$$

This yields an expression for the impulse response

$$\bar{h}_k(t) = (-1)^k R_s \frac{\prod_1^{n-k}{}_j [a - x_j^{(n-k)}]}{\prod_1^n{}_m [a - y_m^{(n)}]} \cdot \left\{\delta(t) - \sum_1^n \frac{P_k[\bar{B}_m^{(n)}]\, e^{\bar{B}_m^{(n)} t}}{\prod_{1}^{n}{}_{j\neq m} [\bar{B}_m^{(n)} - \bar{B}_j^{(n)}]}\right\}, \tag{A19}$$

where $\bar{B}_m^{(n)}$ is as defined in the text.

APPENDIX B

In this appendix we give details of the solution of text Eq. 23, the general equation describing the voltage distribution through the two dimensional network. The equation to solve is

$$A_1\dot{V} + \dot{V}A_1 = A_2V + VA_2 + \frac{\tau E}{g_1} + \frac{\dot{E}}{g_1}, \tag{B1}$$

where A_1, A_2, V, E, τ, g_1 are as defined in the text. Taking the Laplace transform of Eq. B1

$$A_1sV(s) + sV(s)A_1 = A_2V(s) + V(s)A_2 + \frac{(\tau + s)}{g_1}E(s) \tag{B2}$$

or

$$(A_1s - A_2)V(s) + V(s)(A_1s - A_2) = \frac{\tau + s}{g_1}E(s). \tag{B3}$$

Now, writing $g_0 = g_1 + g_2$;

$$\begin{aligned}(A_1s - A_2) &= \left[\frac{s}{2}\left(1 + \frac{4}{R_sg_1}\right) + \frac{\tau}{g_1R_s}\left(\frac{R_2g_0}{2} + 2\right)I \right.\\ &\quad \left. - \left(\frac{s}{R_sg_1} + \frac{\tau}{g_1R_s}\right)D\right]\\ &= -\frac{s+\tau}{R_sg_1}\left\{\left[\frac{s(R_sg_1 + 4) + \tau R_sg_0 + 4\tau}{2(s+\tau)}\right]I + D\right\}\\ &= -\frac{(s+\tau)}{R_sg_1}\bar{D},\end{aligned} \tag{B4}$$

where

$$\bar{D} = \begin{pmatrix} d10 & 0 & & \\ 1d1 & & & \\ 01d & & & \\ & & d10 & \\ & & 1d1 & \\ 0 & & 01d & \end{pmatrix}$$

and $d = [s(R_sg_1 + 4) + \tau R_sg_0 + 4\tau]/[2(s+\tau)]$.

Hence,

$$-\frac{s+\tau}{R_sg_m}[\bar{D}V(s) + V(s)\bar{D}] = \frac{s+\tau}{g_m}E(s) \tag{B5}$$

or

$$[\bar{D}V(s) + V(s)\bar{D}] = -R_sE(s). \tag{B6}$$

The eigenvalues of the matrix $\bar{D}$ are the roots of $S_{2n+1}(\mathrm{d} - \lambda)$ and are

$$\lambda_{2n+1}^{(i)} = d - 2\cos\frac{i\pi}{2n+2} = \mathrm{d} - x_i^{(2n+1)} \tag{B7}$$

$$(i = 1, \ldots, 2n+1).$$

Because $\lambda_{2n+1}^{(i)}$ are real, distinct, and negative by theorem 8.5.1 (Lancaster, 1969), the solution of Eq. B7 is

$$V(s) = R_s\int_0^{+\infty} e^{\bar{D}t}E(s)e^{\bar{D}t}dt. \tag{B8}$$

Now the matrix $\bar{D}$ can be diagonalized as shown in Appendix C. Thus $\bar{D} = T\tilde{D}T^{-1}$, where $\tilde{D}$ is a diagonal matrix. Then $e^{\bar{D}t}$ becomes $e^{\bar{D}t} = Te^{\tilde{D}t}T^{-1}$, where

$$e^{\tilde{D}t} = \begin{pmatrix} e^{\lambda_{2n+1}^{(1)}t}0 & 0 & \cdots\cdots 0 \\ 0 & e^{\lambda_{2n+1}^{(2)}t}0 & \cdots\cdots 0 \\ 0 & 0 & e^{\lambda_{2n+1}^{(3)}t}\cdots\cdots 0 \\ \vdots & \vdots & \vdots \\ 0 & 0 & \cdots\cdots e^{\lambda_{2n+1}^{(2n+1)}t} \end{pmatrix}.$$

Thus Eq. B8 becomes

$$V(s) = R_s\int_0^{+\infty} Te^{\tilde{D}t}T^{-1}E(s)\,Te^{\tilde{D}t}T^{-1}\,dt. \tag{B9}$$

In order to compute the integral, we let $T = (a_{i,j})$ and $T^{-1}(b_{i,j}) = (a_{j,i})$, $e^{\tilde{D}t} = (\lambda_i$ when $i = j$, and 0 when $i \neq j)$, and $E(s) = [J(s)$, when $i = j = n + 1$, and 0 elsewhere]. Because of the form of $E(s)$, $J(s)$ can be brought outside the integral and Eq. B9 becomes

$$V(s) = R_s J(s) \int_0^{+\infty} T\, e^{\tilde{D}t}\, T^{-1}\, \overline{E}\, T\, e^{\tilde{D}t}\, T^{-1}\, dt, \quad \text{(B9a)}$$

where $\overline{E} = [1$, when $i = j = n + 1$; and 0 elsewhere]. Now

$$T^{-1}\,\overline{E} = ({}^1x_{i,j}) = (b_{i,n+1}, \text{ when } j = n + 1, 0 \text{ when } j \neq 0)$$

$$T^{-1}\,\overline{E}\,T = ({}^2x_{i,j}) = (b_{i,n+1}\, a_{n+1,j})$$

$$e^{\tilde{D}t}\,T^{-1}\,\overline{E}\,T = ({}^3x_{i,j}) = (\lambda_i b_{i,n+1}\, a_{n+1,j})$$

$$e^{\tilde{D}t}\,T^{-1}\,\overline{E}\,T\,e^{\tilde{D}t} = ({}^4x_{i,j}) = (\lambda_i b_{i,n+1}\, a_{n+1,j}\,\lambda_j)$$

$$T\,e^{\tilde{D}t}\,T^{-1}\,\overline{E}\,T\,e^{\tilde{D}t} = ({}^5x_{i,j}) = \left(\sum_1^{2n+1} {}_p\, a_{i,p}\, {}^4x_{p,j}\right)$$

and

$$T\,e^{\tilde{D}t}\,T^{-1}\,\overline{E}\,T\,e^{\tilde{D}t}\,T^{-1} = ({}^6x_{i,j}) = \left(\sum_1^{2n+1} {}_q\, {}^5x_{i,q}\, b_{q,j}\right).$$

This can be shown to be equal to

$$\left\{\sum_1^{2n+1}{}_q \sum_1^{2n+1}{}_p\, \lambda_p\lambda_q a_{i,p} a_{j,q} a_{n+1,p} a_{n+1,q}\right\} \quad \text{(B10)}$$

and hence

$$V_{h,k}(s) = R_s J(s) \int_0^{\infty} \sum_1^{2n+1}{}_q \sum_1^{2n+1}{}_p\, \tilde{a}_{h,k,q,p}\, e^{[2d - x_{2n+1}^{(p)} - x_{2n+1}^{(q)}]t}\, dt, \quad \text{(B11)}$$

where $a_{h,k,q,p} = a_{h,p} \cdot a_{k,q} \cdot a_{n+1,p} \cdot a_{n+1,q}$. Now, if we examine the exponent of Eq. B11, we find

$$2d - x_{2n+1}^{(p)} - x_{2n+1}^{(q)}$$

$$= -\left[\frac{s(R_s g_1 + 4) + 4\tau + \tau g_0 R_s}{s + \tau} + x_{2n+1}^{(p)} + x_{2n+1}^{(q)}\right]$$

$$= -\frac{R_s g_1 + 4 + x_{2n+1}^{(p)} + x_{2n+1}^{(q)}}{s + \tau}(s + Y_{2n+1}^{p,q}), \quad \text{(B12)}$$

where

$$Y_{2n+1}^{(p,q)} = \frac{\tau[4 + g_0 R_s + x_{2n+1}^{(p)} + x_{2n+1}^{(q)}]}{4 + R_s g_1 + x_{2n+1}^{(p)} + x_{2n+1}^{(q)}}.$$

It can easily be shown that $2d - x_{2n+1}^{(p)} - x_{2n+1}^{(q)} < 0$ and so

$$V_{h,k}(s) = -R_s J(s) \sum_1^{2n+1}{}_q \sum_1^{2n+1}{}_p$$

$$\frac{\tilde{a}_{h,k,q,p}}{4 + R_s g_1 + x_{2n+1}^{(p)} + x_{2n+1}^{(q)}}\left[1 + \frac{\tau - Y_{2n+1}^{(p,q)}}{s + Y_{2n+1}^{(p,q)}}\right]. \quad \text{(B13)}$$

If $J(s)$ is dropped from Eq. B13, the right-hand side of the equation defines the Laplace transform of the network impulse response $h_{h,k}(t)$. Taking the inverse transform, we obtain

$$h_{h,k}(t) = -R_s \sum_1^{2n+1}{}_q \sum_1^{2n+1}{}_p$$

$$\cdot\, \tilde{b}_{h,k,q,p}[\delta(t) + [\tau - Y_{2n+1}^{(p,q)}]e^{-Y_{2n+1}^{(p,q)} t}], \quad \text{(B14)}$$

where $\tilde{b}_{h,k,q,p} = (\tilde{a}_{h,k,q,p})/[4 + R_s g_1 + x_{2n+1}^{(p)} + x_{2n+1}^{(q)}]$. Eq. B14 is the required solution for the two-dimensional network.

APPENDIX C

In this appendix, we describe the diagonalization of matrix A.

$$A = \begin{pmatrix} a1 & 0 & & & \\ 1a & 1 & 0 & & \\ 0 & 1a & & & \\ & & a1 & 0 & \\ & 0 & 1 & a & \\ & & 0 & 1a & \end{pmatrix}, \quad \text{(C1)}$$

where A is a $n \times n$ matrix. We will also find an orthonormal matrix T such that $A = T\tilde{A}\,T^{-1}$, where $\tilde{A}$ is diagonal and $T^{-1} = T^*$, where T^* is the transpose of T.

The eigenvalues of A are the roots of the Chebyshev polynomials $S_n(a-\lambda)$. Because the roots of Chebyshev polynomials are real and simple, the eigenvalues, $\lambda_m^{(n)}$, of A are also real and simple and are defined by

$$\lambda_m^{(n)} = a - 2\cos\frac{m\pi}{n+1} \quad \text{(C2)}$$

$$= a - x_m^{(n)},$$

where $m = 1, \ldots n)$.

We now find the eigenvectors, $|x_m^{(n)}|$, of A_n associated with $\lambda_m^{(n)}$. We first define the eigenvector

$$|x_m^{(n)}| = \begin{pmatrix} x_{1,m}^{(n)} \\ x_{2,m}^{(n)} \\ \vdots \\ x_{n,m}^{(n)} \end{pmatrix}. \quad \text{(C3)}$$

We can then write

$$A|x_m^{(n)}| = \lambda_m^{(n)}|x_m^{(n)}|. \quad \text{(C4)}$$

Eq. C4 defines a homogeneous system of n equations in n variables, thus

$$x_{1,m}^{(n)} a + x_{2,m}^{(n)} = \lambda^{(n)}_m\, x_{1,m}^{(n)},$$

$$x_{1,m}^{(n)} + a x_{2,m}^{(n)} + x_{3,m}^{(n)} = \lambda^{(n)}_m\, x_{2,m}^{(n)},$$

$$\vdots \qquad\qquad \vdots$$

$$x_{n-2,m}^{(n)} + a x_{n-1,m}^{(n)} + x_{n,m}^{(n)} = \lambda^{(n)}_m\, x_{n-1,m}^{(n)},$$

$$x_{n-1,m}^{(n)} + a x^{(n)}{}_{n,m} = \lambda^{(n)}{}_m\, x^{(n)}_{n,m}.$$

The solution of Eq. C4 is

$$\alpha_m \cdot \begin{pmatrix} S_0[-x_m^{(n)}] \\ S_1[-x_m^{(n)}] \\ \vdots \\ S_{n-1}[-x_m^{(n)}] \end{pmatrix}, \quad \text{(C5)}$$

where $\alpha_m \neq 0$ is an arbitrary constant. α_m can be chosen so that $||x_m^{(n)}|| = 1$; i.e., $|x_m^{(n)}|$ is normal. Then

$$\alpha_m = \frac{1}{\sqrt{\sum_i^n S_{i-1}^2 [-x_m^{(n)}]}}. \tag{C6}$$

The matrix T formed with columns equal to $|x_m^{(n)}|$:

$$T = (t_{i,j}) = \alpha_j S_{i-1} [-x_j^{(n)}] \tag{C7}$$

is an orthonormal matrix because eigenvectors associated with distinct eigenvalues are orthogonal and because the eigenvectors have been normalized. Thus, $T^{-1} = T$.

From Eqs. C6 and C7, we write

$$t_{i,j} = \frac{S_{i-1} [-x_j^{(n)}]}{\sqrt{\sum_p^n S_{p-1}^2 [-x_j^{(n)}]}}. \tag{C8}$$

Now, $S_k[-2\cos(h\pi/n+1)] = U_k[-\cos(h\pi/n+1)]$ (theorem 22.5.13 of Abramowitz and Stegun, 1964). But $U_k(\cos\phi) = \sin\{[(k+1)\phi]/\sin\phi\}$ (theorem 22.3.16 of Abramowitz and Stegun, 1964), and so

$$V_k\left(-\cos\frac{h\pi}{n+1}\right) = V_k\left[\cos\left(\frac{h\pi}{n+1}+1\right)\pi\right] = \frac{\sin\left[(k+1)\left(\frac{h}{n+1}+1\right)\pi\right]}{\sin\left(\frac{h}{n+1}+1\right)\pi}.$$

It is easy to see that

$$\sin\left[(k+1)\left(\frac{h}{n+1}+1\right)\pi\right] = (-1)^{k+1}\sin\frac{h(k+1)\pi}{n+1}$$

and

$$\sin\left(\frac{h}{(n+1)}+1\right)\pi = -\sin\frac{h\pi}{n+1}.$$

Thus,

$$S_k(-x_h^{(n)}) = (-1)^k \frac{\sin\frac{h(k+1)\pi}{n+1}}{\sin\frac{h\pi}{n+1}}. \tag{C9}$$

And hence

$$t_{i,j} = \frac{S_{i-1}[-x_j^{(n)}]}{\sqrt{\sum_p^{2n+1} S_{p-1}^2[-x_j^{(n)}]}} = \frac{(-1)^{i-1}\sin\frac{ij\pi}{n+1}}{\sqrt{\sum_p^n S_{p-1}^2[-x_j^{(n)}]}}$$

or, using theorem 1.351 of Gradshteyn and Ryzhik (1965)

$$t_{i,j} = \frac{(-1)^{i-1}\sin\frac{ij\pi}{n+1}}{\sqrt{\frac{n}{2} - (-1)^j \frac{\sin\frac{nj\pi}{n+1}}{2\sin\frac{j\pi}{n+1}}}}. \tag{C10}$$

APPENDIX D

In this appendix, the inversion of matrix A (see text, Eq. 8) and $\overline{A}$ (text, Eq. 9) is described in detail. A_n is an $n \times n$ matrix of the type

$$A_n = \begin{pmatrix} a1 & 0 & & & \\ 1a & 1 & 0 & & \\ 0 & 1a & & & \\ & & a & 1 & 0 \\ & & 1 & a & 1 \\ & 0 & & 1 & a \end{pmatrix} \tag{D1}$$

$S_n(a)$ is the determinant of the matrix A_n. It is easy to prove that

$$S_{n+1}(a) = aS_n(a) - S_{n-1} \text{ for } n \geq 1, \tag{D2}$$

where $S_1(a) = a$, $S_0(a) = 1$, and

$$S_n(a) = S_j(a)S_{n-j}(a) - S_{j-1}(a)S_{n-j-1} \text{ for } 1 \leq j \leq n. \tag{D3}$$

It is important to note that Eq. D2 implies that $S_n(a)$ defines an orthogonal set of Chebyshev polynomials of the second kind (theorem 22.7.6 of Abramowitz and Stegun, 1964). This makes it easy to prove that

$$A_n^{-1} = (a_{j,k}) \text{ where } a_{j,k} = \frac{1}{S_n(a)}(-1)^{j+k}S_{j-1}(a)S_{n-k}(a) \text{ for } j \leq k$$

and

$$a_{j,k} = \frac{1}{S_n(a)}(-1)^{j+k}S_{k-1}(a)S_{n-j}(a) \text{ for } j \geq k. \tag{D4}$$

This follows from the definition of an inverted matrix and can be verified by showing that $A \cdot A^{-1} = 1$. Eq. D2 also implies that

$$S_n(x) = \prod_m^n \left(x - 2\cos\frac{m\pi}{n+1}\right), \tag{D5}$$

i.e., the zeroes of $S_n(x)$ are real and simple. Eq. D4 is the required inversion of matrix A.

The matrix $\overline{A}$ is also an $n \times n$ matrix of the type

$$\overline{A}_n = \begin{pmatrix} a2 & 0 & & & \\ 1a & 1 & 0 & & \\ 0 & 1a & & & \\ 0 & 1 & a & & \\ & & & a & 1 & 0 \\ & & & 1 & a & 1 \\ & & 0 & & 1 & a \end{pmatrix}. \tag{D6}$$

It is easily proved that if $C_n(a)$ is the determinant of $\overline{A}_n$, then

$$C_{n+1}(a) = aC_n(a) - C_{n-1}(a) \text{ for } n \geq 1 \tag{D7}$$

and $C_1(a) = a$, $C_0(a) = 2$, and

$$C_n(a) = S_j(a)C_{n-j}(a) - S_{j-1}(a)C_{n-j-1}(a). \tag{D8}$$

Eq. D7 implies that $C_n(a)$ is a Chebyshev polynomial of the first kind (theorem 22.7.7 of Abramowitz and Stegun, 1964), and we note that the

zeroes of $C_n(x)$ are therefore real and simple

$$C_n(x) = \prod_1^n{}_n \left[x - 2 \cos \left(\frac{2m-1}{2n} \right) \pi \right]. \qquad \text{(D9)}$$

Thus, it is easy to prove that

$$\bar{A}_n^{-1} = (\bar{a}_{j,k}) = \frac{1}{C_n(a)} \cdot (-1)^{j+k} C_{j-1}(a) S_{n-k}(a) \text{ for } 1 < j \leq k$$

$$= \frac{1}{C_n(a)} \cdot (-1)^{j+1} C_{k-1}(a) S_{n-j}(a) \text{ for } j \geq k$$

$$= \frac{1}{C_n(a)} \cdot (-1)^{k+1} S_0(a) S_{n-k}(a) \text{ for } j = 1.$$

REFERENCES

Abramowitz, M., and I. A. Stegun. 1964. Handbook of Mathematical Functions. Dover Pubns., Inc., New York.

Attwell, D., and M. Wilson, 1980. Behaviour of the rod network in the tiger salamander retina mediated by membrane properties of individual rods. *J. Physiol. (Lond.)* 309:287–315.

Baylor, D. A., and A. L. Hodgkin. 1973. Detection and resolution of visual stimuli by turtle photoreceptors. *J. Physiol. (Lond.).* 234:163–198.

Baylor, D. A., M. G. F. Fuortes, and P. M. O'Bryan. 1971. Receptive fields of cones in the retina of the turtle. *J. Physiol. (Lond.).* 214:265–294.

Baylor, D. A., A. L. Hodgkin, and T. D. Lamb. 1974. Reconstruction of the electrical responses of turtle cones to flashes and steps of light. *J. Physiol. (Lond.).* 242:759–791.

Baylor, D. A., T. D. Lamb, and K.-W. Yau. 1979. Responses of retinal rods to single photons. *J. Physiol (Lond.).* 288:613–634.

Bendat, J. S., and A. G. Piersol. 1971. *Random Data: Analysis and Measurement Procedures.* John Wiley and Sons, Inc., New York.

Brown, K. T., and D. G. Flaming. 1977. New microelectrode techniques for intracellular work on small cells. *Neuroscience.* 2:813–827.

Cole, K. S., and R. F. Baker. 1941. Transverse impedance of the squid giant axon during current flow. *J. Gen. Physiol.* 24:535–549.

Copenhagen, D. R., and W. G. Owen. 1976*a*. Coupling between rod photoreceptors in a vertebrate. *Nature (Lond.).* 260:57–59.

Copenhagen, D. R., and W. G. Owen. 1976*b*. Functional characteristics of lateral interactions between rods in the retina of the snapping turtle. *J. Physiol. (Lond.).* 259:251–282.

Detwiler, P. B., and A. L. Hodgkin. 1979. Electrical coupling between cones in turtle retina. *J. Physiol. (Lond.).* 291:75–100.

Detwiler, P. B., A. L. Hodgkin, and P. A. McNaughton. 1978. A surprising property of electrical spread in the network of rods in the turtle's retina. *Nature (Lond.).* 274:562–565.

Detwiler, P. B., A. L. Hodgkin, and P. A. McNaughton. 1980. Temporal and spatial characteristics of the voltage response of rods in the retina of the snapping turtle. *J. Physiol. (Lond.).* 300:213–250.

Fain, G. L. 1975. Quantum sensitivity of rods in the toad retina. *Sciences (NY)* 187:838–841.

Fain, G. L. 1976. Sensitivity of toad rods: dependence on wavelength and background illumination. *J. Physiol. (Lond.).* 261:71–101.

Gold, G. H. 1979. Photoreceptor coupling in the retina of the toad, *Bufo marinus.* II. Physiology. *J. Neurophysiol., (Bethesda).* 42:311–328.

Gradshteyn, I. S., and I. M. Ryzhik. 1965. *Tables of Integrals Series and Products.* Academic Press, Inc., New York.

Hodgkin, A. L., and A. F. Huxley. 1952. A quantitative description of membrane current and its application to conduction and excitation in nerve. *J. Physiol. (Lond.).* 117:500–544.

Lamb, T. D., and E. J. Simon. 1976. The relation between intercellular coupling and electrical noise in turtle photoreceptors. *J. Physiol. (Lond.).* 263:257–286.

Lamb, T. D., P. A. McNaughton, and K.-W. Yau. 1981. Spatial spread of activation and desensitization in toad rod outer segments. *J. Physiol. (Lond.).* 319:463–496.

Lancaster, P. 1969. *Theory of Matrices.* Academic Press, Inc., New York.

Schwartz, E. A. 1975. Rod-rod interaction in the retina of the turtle. *J. Physiol. (Lond.).* 246:617–638.

Schwartz, E. A. 1976. Electrical properties of the rod syncitium in the retina of the turtle. *J. Physiol. (Lond.).* 257:379–406.

Werblin, F. S. 1978. Transmission along and between rods in the tiger salamander retina. *J. Physiol. (Lond.).* 280:449–470.